Particulate barium tracing significant mesopelagic carbon remineralisation in the North Atlantic

Nolwenn Lemaitre [1, 2], Hélène Planquette[1], Frédéric Planchon[1], Géraldine Sarthou[1], Stéphanie Jacquet[3], Maribel I. García-Ibáñez[4,5], Arthur Gourain[1, 6], Marie Cheize[1], Laurence Monin[7], Luc André[7], Priya Laha[8], Herman Terryn[8] and Frank Dehairs[2]

[1]Laboratoire des Sciences de l'Environnement Marin (LEMAR), UMR 6539, IUEM, Technopôle Brest Iroise, 29280 Plouzané, France

[2]Vrije Universiteit Brussel, Analytical, Environmental and Geo-Chemistry, Earth System Sciences research group, Brussels, Belgium

[3]Aix Marseille Université, CNRS/INSU, Université de Toulon, IRD, Mediterranean Institute of Oceanography (MIO), UM 110, 13288 Marseille, France

[4]Uni Research Climate, Bjerknes Centre for Climate Research, Bergen 5008, Norway.

[5]Instituto de Investigaciones Marinas, IIM-CSIC, Eduardo Cabello 6, 36208 Vigo, Spain

[6]Ocean Sciences Department, School of Environmental Sciences, University of Liverpool, Liverpool L69 3GP, United Kingdom

[7]Earth Sciences Department, Royal Museum for Central Africa, Leuvensesteenweg 13, Tervuren, 3080, Belgium

[8]Vrije Universiteit Brussel, SURF research group, department of Materials and Chemistry, Brussels, Belgium

Correspondance to: Nolwenn Lemaitre, Department of Earth Sciences, Institute of Geochemistry and Petrology, ETH-Zürich, Zürich, Switzerland. (nolwenn.lemaitre@erdw.ethz.ch)

Keywords: Particulate biogenic barium; Carbon remineralisation; North Atlantic; Biological pump

Abstract

The remineralisation of sinking particles by prokaryotic heterotrophic activity is important for controlling oceanic carbon sequestration. Here, we report mesopelagic particulate organic carbon (POC) remineralisation fluxes in the North Atlantic along the GEOTRACES-GA01 section (GEOVIDE cruise; May-June 2014) using the particulate biogenic barium (excess barium; Ba_{xs}) proxy. Important mesopelagic (100–1000 m) Ba_{xs} differences were observed along the transect depending on the intensity of past blooms, the phytoplankton community structure and the physical forcing, including downwelling. The subpolar province was characterized by the highest mesopelagic Ba_{xs} content (up to 727 pmol L^{-1}), which was attributed to an intense bloom averaging 6 mg Chl-*a* m^{-3} between January and June 2014 and by an intense 1500 m-deep convection in the central Labrador Sea during the winter preceding the sampling. This downwelling could have promoted a deepening of the prokaryotic heterotrophic activity, increasing the Ba_{xs} content.

In comparison, the temperate province, characterized by the lowest Ba_{xs} content (391 pmol L^{-1}), was sampled during the bloom period and phytoplankton appear to be dominated by small and calcifying species, such as coccolithophorids. The Ba_{xs} content, related to an oxygen consumption, was converted into a remineralisation flux using an updated relationship, proposed for the first time in the North Atlantic. The estimated fluxes were in the same order of magnitude than other fluxes obtained by independent methods (moored sediment traps, incubations) in the North Atlantic. Interestingly, in the subpolar and subtropical provinces, mesopelagic POC remineralisation fluxes (up to 13 and 4.6 mmol C m^{-2} d^{-1}, respectively) were equalling and occasionally even exceeding upper ocean POC export fluxes, deduced using the ^{234}Th method. These results highlight the important impact of the mesopelagic remineralisation on the biological carbon pump of the studied area with a near-zero, deep (> 1000 m) carbon sequestration efficiency in spring 2014.

1. Introduction

The ocean represents the largest active CO_2 sink (Sabine et al., 2004) partly materialized by the oceanic biological carbon pump (BCP), which controls the export of carbon and nutrients to the deep ocean through the production of biogenic sinking particles (Boyd and Trull, 2007; Sigman and Boyle, 2000; Volk and Hoffert, 1985). The North Atlantic sustains one of the most productive spring phytoplankton bloom of the world's ocean (Esaias et al., 1986; Henson et al., 2009; Longhurst, 2010; Pommier et al., 2009). The high primary productivity in combination with the water mass formation there as part of the thermohaline circulation (Seager et al., 2002), results in a particularly efficient BCP in the North Atlantic (Buesseler et al., 1992; Buesseler and Boyd, 2009; Herndl and Reinthaler, 2013; Honjo and Manganini, 1993; Le Moigne et al., 2013b), estimated to contribute up to 18% of the global oceanic BCP (Sanders et al., 2014). However, the magnitude of the carbon transfer to the deep ocean depends on many factors including the efficiency of bacterial remineralisation within the mesopelagic layer (100–1000 m depth layer). In this layer, most of the particulate organic carbon (POC) exported from the upper mixed layer is respired or released to the dissolved phase as dissolved organic carbon (DOC; Buesseler et al., 2007; Buesseler and Boyd, 2009; Burd et al., 2016; Herndl and Reinthaler, 2013; Lampitt and Antia, 1997; Martin et al., 1987). Mesopelagic remineralisation has been often reported to balance or even exceed the carbon supply from the surface (i.e. POC and DOC; Aristegui et al., 2009; Baltar et al., 2009; Burd et al., 2010; Collins et al., 2015; Fernández-castro et al., 2016; Giering et al., 2014; Reinthaler et al., 2006), highlighting the impact of mesopelagic processes on bathypelagic carbon sequestration. Unfortunately, studies focusing on the mesopelagic layer are scarce, and the remineralisation process in this part of the water column remains poorly constrained. A variety of methods have been used to assess deep remineralisation. The attenuation of the particulate organic matter concentration with depth can be deduced from POC fluxes recorded by bottom tethered or free-floating neutrally buoyant sediment traps (e.g., Buesseler et al., 2007; Honjo et al., 2008; Martin et al., 1987) deployed at different depths. Bacterial respiration can be assessed by measuring the rate of dissolved oxygen consumption, but this approach is usually limited to the upper 200 m of depth because of sensitivity issues (Arístegui et al., 2005; Christaki et al., 2014; Lefèvre et al., 2008). However, sediment traps and direct respiration measurements are insufficiently reliable for depths exceeding 200 to 500 m (i.e. the lower mesopelagic area). Earlier work has revealed that the accumulation of particulate biogenic barium (excess barium; Ba_{xs}) in the mesopelagic water column (100 – 1000 m) is related with organic carbon remineralisation. This biogenic Ba is essentially carried by barite

($BaSO_4$) micro-crystals, which form inside oversaturated micro-environments, mostly aggregates of organic material where prokaryotic activity is intense (Bishop, 1988; Collier and Edmond, 1984; Dehairs et al., 1980; Ganeshram et al., 2003; Gonzalez-Munoz et al., 2003). Bacterial activity will result in the disruption of these aggregates, thereby releasing the barite crystals in the ambient water. As a result, the concentration of Ba_{xs} relates with oxygen consumption rate (Dehairs et al., 1997; Shopova et al., 1995) and can be converted into a remineralisation rate of POC in the mesopelagic layer (Dehairs et al., 1997). Ba_{xs} has been successfully used as a proxy of POC remineralisation flux in the Southern Ocean (Cardinal et al., 2005; Jacquet et al., 2008a, 2008b, 2011a, 2015; Planchon et al., 2013) and Pacific Ocean (Dehairs et al., 2008).

We examined mesopelagic POC remineralisation along the GEOTRACES-GA01 section during the GEOVIDE cruise (15 May–30 June, 2014; R/V Pourquoi Pas?) by assessing particulate biogenic barium (excess barium; Ba_{xs}) contents. This study is the first one to report the use of the Ba_{xs} proxy in the North Atlantic. Regional variations of the Ba_{xs} distributions along the crossed biogeochemical provinces are discussed regarding the stage and intensity of the bloom, the phytoplankton community structure and the physical forcing. We re-assessed the algorithm between Ba_{xs} content and oxygen consumption developed for the Southern Ocean, adapting it for the North Atlantic. We compared the remineralisation fluxes resulting from this new North Atlantic-specific algorithm with those obtained by other methods in the same area. This comparison, in combination with surface primary production (PP) and POC export estimates (Lemaitre et al., 2018; this issue), allowed us to evaluate the fate of POC to the deep ocean and to constrain the BCP in the North Atlantic.

2. Methods

2.1. Study area

The GEOVIDE section (15 May–30 June 2014; R/V Pourquoi pas?) crossed different biogeochemical provinces in the North Atlantic including the North Atlantic subtropical gyre (NAST; Stations 1 and 13), the North Atlantic drift (NADR) covering the West European (Stations 21 and 26) and Icelandic (Stations 32 and 38) basins, and the Atlantic Arctic (ARCT) divided between the Irminger (Stations 44 and 51) and Labrador (Stations 64, 69 and 77) Seas (Longhurst, 1995; Fig. 1, 2).

The evolution of chlorophyll-*a* (Chl-*a*) concentrations from satellite imagery (Fig. 1) revealed the decline of the bloom in the NAST and the Labrador Sea and the bloom period within the NADR province and the Irminger Sea. Indeed, the highest daily PP rates were measured in the NADR and in the Irminger Sea (> 150 mmol C m^{-2} d^{-1}; Fonseca-Batista et al., 2018; this issue; Lemaitre et al., 2018; this issue). The phytoplankton community structure also varied regionally, with diatoms dominating the ARCT province and the West European basin of the NADR, coccolithophorids dominating the Icelandic basin of the NADR and cyanobacteria in the NAST province (Tonnard et al., 2018; this issue). Finally, as described elsewhere (Daniault et al., 2016; García-Ibáñez et al., 2015; Kieke and Yashayaev, 2015; Zunino et al., 2017; this issue), these provinces also differ in terms of their hydrographic features. The NADR province is crossed by the sub-arctic front (SAF), which was located near Station 26 during GEOVIDE (Fig. 2). Strong currents were observed near the Greenland margin (probably influencing Stations 51 and 64), and an intense 1500 m-deep convection happened during the winter preceding GEOVIDE in the central Labrador Sea (Station 69) due to the

formation of the Labrador Sea Water (LSW) in winter (Fig. 2). These features influenced the magnitude of the carbon export fluxes, as well as the export and transfer efficiencies along the transect (Lemaitre et al., 2018; this issue). The highest POC export fluxes from the upper-ocean (calculated at the depth "z" ranging from 40 to 130 m at Station 44 and 32, respectively) were observed in the NADR province and in the Labrador Sea and reached up to 10 mmol C m^{-2} d^{-1} at Station 69 (Lemaitre et al., 2018; this issue). Export efficiency (i.e., the ratio of the POC export over the PP) was generally low (≈10%), except at Stations 1 and 69 where it reached 30%. The transfer efficiency (defined as the ratio of the POC export at z+100 m over the POC export at z) was more variable, ranging from 30% at Station 69 to 92% at Station 26 (Lemaitre et al., 2018; this issue).

2.2. Sampling and analyses

For different objectives, during GEOVIDE, suspended particles were collected by different sampling techniques. The main goal of the Niskin sampling was to derive Ba_{xs} concentrations and, thus, carbon remineralisation fluxes in the mesopelagic zone (high resolution in the 100-1000 m layer) at stations where PP data and carbon export fluxes were also determined. The goal of the Go-Flo sampling was, at first, dedicated to the determination of all dissolved and particulate trace elements and their isotopes. Since particulate Ba and Al were determined on samples collected by both sampling techniques, we took the opportunity to compare both datasets in order to assess the quality of our data.

1) Ba_{xs} concentrations measured in samples collected using a standard CTD rosette equipped with 12 L Niskin bottles. At eleven station, 18 depths were generally sampled between the surface and 1500 m in order to cover a high vertical resolution in the mesopelagic layer (Table S1).

Four to 8 L of seawater were filtered on acid-cleaned polycarbonate membranes of 0.4 µm porosity (Nuclepore®, 47 or 90 mm diameter). Filter membranes were rinsed with Milli-Q grade water (18.2 MΩ cm; ≤ 5 mL) to remove sea-salt, dried at ambient temperature under a laminar flow hood and finally stored in clean petri slides until analysis in the home based laboratory.

Filters were totally digested overnight with a concentrated tri-acid mixture (1.5 mL HCl / 1 mL HNO_3 / 0.5 mL HF; all Merck suprapur grades) using clean Teflon vials (Savillex®) on a hot plate at 90°C. The acid solution was then evaporated at 110°C until near dryness and the residue dissolved in 13 mL 0.32M HNO_3 (Merck; distilled Normapur). The solutions were transferred to polypropylene tubes (VWR) and analysed for Barium (Ba), Aluminium (Al) and other major and minor elements using an inductively coupled plasma-quadrupole mass spectrometer (ICP-QMS; X Series 2 Thermo Fisher) equipped with a collision cell technology (CCT). We used a concentric quartz nebulizer (1 mL min^{-1}) and nickel sample and skimmer cones. During the analyses, internal standards (Ru, In, Re and Bi) were added to samples in order to monitor and correct the instrumental drift and matrix-dependent sensitivity variations.

Two multi-element artificial standard solutions were prepared for external calibration. The first contained major elements (Na, Mg, Al, Ca and Ti) and the second was prepared with minor elements (Sr, Ba, REEs, Th and U). Standards were prepared by dilution of the multi-element mixed standard stock solutions to span the expected range of sample concentrations, with concentrations in the standard curve spaced to cover potential sample variations.

The accuracy and precision of our analyses were assessed using the following Certified Reference Materials (CRM): BHVO-1, JB-3, JGb-1 and SLRS-5 (Table 1).

The detailed procedure for sample preparation and analysis is given in Cardinal et al. (2001).

2) Ba_{xs} concentrations measured in samples collected using the trace metal clean rosette, equipped with twenty-two 12 L Go-Flo bottles at higher spatial resolution (31 stations) but with lower vertical resolution in the mesopelagic layer. Details about filtration, sample processing and analyses can be found in Gourain et al. (2018; this issue). Briefly, at each depth, two size fractions were investigated: 0.45–5 µm using polysulfone filters (Supor®) and > 5 µm using mixed ester cellulose filters (MF, Millipore®). Between 2 and 5 L of seawater were filtered for the upper water column (surface to 100 m) and 10 L for depths exceeding 100 m. Excess seawater from the filters was drawn off and then the filters were frozen in acid-cleaned petri-dishes until home analysis. In the laboratory, filters were digested with a solution of 8 M HNO_3 (Ultrapur grade, Merck) and 2.3 M HF (Suprapur grade, Merck). Vials were then refluxed at 130 °C on a hotplate for 4 h. After gentle evaporation, the residue was redissolved with approximately 2 mL of 0.32 M HNO_3 spiked with 1 µg L^{-1} of Indium. Solutions were analysed using a SF-ICP-MS (Element 2, Thermo) following the method of Planquette and Sherrell (2012). Total Ba and Al concentrations were calculated by summing the two size fractions. The accuracy and precision of these analyses were assessed using the BCR-414 CRM (see Gourain et al., 2018; this issue).

For both Niskin and Go-Flo samples, the Ba_{xs} concentrations were calculated by subtracting the particulate lithogenic barium (pBa-litho) from the total particulate barium (pBa). The pBa-litho was determined by multiplying the particulate aluminium (pAl) concentration by the upper continental crust (UCC) Ba:Al molar ratio (0.00135 mol mol^{-1}; Taylor and Mclennan, 1985). Along the GEOVIDE section, the pBa-litho fraction represented less than 7 % of total barium, except at Stations 1 and 53, close to the Iberian and Greenland margin where pBa-litho accounted for 28 and 44 % of total Ba, respectively. Because of the rather large uncertainty associated with the UCC Ba:Al ratio and because of the high lithogenic particle loads at Stations 1 and 53, those stations were not considered further in this study. Uncertainties on Ba_{xs} concentrations were estimated using error propagation and ranged between 6 and 25 %.

For stations where total pBa and pAl concentrations were available at similar depths, the regression of Ba_{xs} concentrations (100-1000 m layer) from the Go-Flo samples vs. those of the Niskin samples was significant (regression slope: 0.87; R^2: 0.61; $p<0.01$; n=66; Fig. S1) despite some discrepancies, especially in the higher concentration domain. Such discrepancies could have resulted from differences in the chemical protocols and most likely the filters used. The Niskin samples collected on 0.4 µm polycarbonate filters were digested using a tri-acid mix (50% HCl/33% HNO_3/17% HF), while the Go-Flo samples collected on paired 0.45 µm polyestersulfone / 5 µm mixed ester cellulose filters were digested using a 50% HNO_3/10% HF acid mix. The use of different filter types has been shown to lead to different concentrations, depending on the element of consideration, despite using the same digestion technique (Planquette and Sherrell, 2012). The addition of HCl has been shown to not improve elemental recoveries of marine particles (Ohnemus and Lam, 2014) but the larger HF concentration of the tri-acid mix used for digesting the Niskin samples, likely, dissolved more of the refractory particles, explaining the slightly higher concentrations obtained for these samples.

In addition, filtered suspended matter was also analysed using a Field Emission Scanning Electron Microscope (FE-SEM; JEOL JSM-7100F) to detect the presence of barite particles. Because of time consuming analyses, seven filters from the different basins were scanned: six samples with high mesopelagic Ba_{xs} concentrations (Station 13 at 400 m; Station 38 at 300 m; Station 44 at 300 and 700 m; Station 69 at 600 m and Station 77 at 300 m) and one sample with high surface Ba_{xs} concentrations (Station 26 at 50 m). For each sample, a filter surface of 0.5 cm^2 was analysed.

To verify the relationship between Ba_{xs} and barite particles (see section 4.1), we evaluated the contribution of the barite particles to Ba_{xs} concentrations for the sample collected at 600 m at Station 69 and which has a high mesopelagic Ba_{xs} content (see Section 3). Using the FE-SEM, 0.003% of the total filter surface was scanned and size and volume of all detected barite particles present in this surface area were assessed. To this aim, each barite particle was pictured using a magnification setting between 12,000 and 15,000×. Images were then analysed with the software ImageJ and, for each barite particle, the longest and shortest axes were measured and pixels were converted to nanometres. Barite particles were then assimilated to ellipses to calculate their volume. Finally, the concentration of pBa of each barite particle was calculated using Eq. (1):

$$\text{pBa in barite} = \Sigma \left[V \times \mu_{BaSO4} \times (M_{Ba} / M_{BaSO4}) \right] / V_{SW} \quad (1)$$

where V is the volume of the barite particle (between 0.01 and 3.96 μm^3), μ_{BaSO4} is the density of barite (4.45 g cm^{-3}), M_{Ba} / M_{BaSO4} is the molar proportion of barium in $BaSO_4$ (0.59) and V_{SW} is the volume of seawater filtered (equivalent to 0.2 mL for the portion of filter surface analysed).

3. Results

3.1. Particulate biogenic Ba_{xs} distribution

3.1.1. Section overview

The Ba_{xs} longitudinal section of concentrations (Fig. 4) shows elevated concentrations between 100 and 1000 m, in the mesopelagic layer (333 ± 224 pmol L^{-1}; median ± 1s.d.; n=209). In comparison, the surface ocean (depths < 100 m) and the deep ocean (depths > 1000 m) are characterized by lower median values (94 and 114 pmol L^{-1}, n=113 and 199, respectively). Exceptions can be observed for the upper waters at Stations 25 and 26 and bottom waters at Stations 29, 32, 36, 38 and 71 where high Ba_{xs} concentrations may be attributed to Ba assimilation by phytoplankton and sediment resuspension, respectively (Gourain et al., 2018; this issue). Concentrations ranged from 4 (Station 11, 55 m) to 24643 (Station 26, 35 m) pmol L^{-1} in surface waters and from 7 (Station 71, 350 m) to 1388 (Station 15, 300 m) pmol L^{-1} in the mesopelagic layer (100–1000 m). For the mesopelagic layer, where the maximum Ba_{xs} concentrations were generally observed, the highest Ba_{xs} concentration was observed in the NAST province, reaching 1388 pmol L^{-1} at 300 m of Station 15. These maxima occurred between 200 and 600 m but were spread over larger depth intervals in the ARCT province, where high Ba_{xs} values occurred until 1200 m depth at Station 69.

3.1.2. Individual Profiles

In this section, we only present Ba_{xs} concentrations obtained from Niskin bottles. This is because (i) both data sets converge (regression slope: 0.87; R^2: 0.61; $p<0.01$; n=66); (ii) Niskin casts had a better sampling resolution in the 100–1000 m layer; and (iii) Niskin casts were also used for the determination of POC export using the 234-Th deficit method (see Lemaitre et al., 2018; this issue).

All the vertical Ba_{xs} profiles (Fig. 5) show increased concentrations between 100 and 1000 m, followed by lower concentrations deeper that tend to return to a background level of 180 ± 54 pmol L^{-1} (n=10) as average along the GEOVIDE transect. This background value is quite characteristic for the deep ocean (> 1000 m) and is considered to

represent the residual Ba_{xs} left over after partial dissolution and sedimentation of Ba_{xs} produced during previous phytoplankton growth events (Dehairs et al., 1997).

In the NAST province (Station 13), the Ba_{xs} concentrations steadily increased from the surface to 400 m, reaching 961 pmol L^{-1}, then decreased with depth, reaching the background level of 180 pmol L^{-1} at 1500 m.

In the West European basin of the NADR province, vertical profiles of Ba_{xs} were similar, yet concentrations in the mesopelagic layer were smaller at Station 21 with Ba_{xs} peaking only at 524 pmol L^{-1}. Ba_{xs} concentrations returned to the background value at 1200 m. Ba_{xs} concentration in surface waters of Station 26 were the highest of the entire section reaching 1888 pmol L^{-1} at 50 m (note that the value for the Go-Flo sample at 35 m reaches 24643 pmol L^{-1}; section 3.1.1). Below this depth, Ba_{xs} concentrations decreased back to the background level at 100 m, then increased again, with a second peak of 451 pmol L^{-1} at 200 m. In the Icelandic basin of the NADR province, Ba_{xs} concentrations were relatively high, reaching 646 and 711 pmol L^{-1} at 200 and 300 m at stations 32 and 38, respectively. Station 38 was also characterized by a double Ba_{xs} peak at 300 and 700 m. Below this second maximum, Ba_{xs} concentrations decreased to the background level at 1000 m for both stations.

In the ARCT province, a similar double peak profile was observed at Station 44, in the Irminger Sea, with Ba_{xs} concentrations reaching 750 pmol L^{-1} between 200 and 400 m and 820 pmol L^{-1} at 700 m. Then, Ba_{xs} concentrations returned to the background value at 1100 m. Close to the Greenland margin (Station 51), Ba_{xs} concentrations reached a maximum of 495 pmol L^{-1} at 300 m, which was lower than the maxima determined at the other stations of the ARCT province.

The Ba_{xs} concentrations of Stations 44 and 51 were compared to those obtained at Station 11 (63.5°N–324.8°E) and Station 5 (56.9°N–317.2°E) of the GEOSECS cruise, in summer 1970 (Brewer et al., unpublished results; Fig. 5). The Ba_{xs} concentrations obtained at GEOSECS Station 11 vary over a similar range as those for GEOVIDE Station 44 (173–658 pmol L^{-1} and 116–823 pmol L^{-1}, respectively). Similar ranges were also observed between GEOSECS Station 5 and GEOVIDE Station 51 (170–402 pmol L^{-1} and 127–359 pmol L^{-1}, respectively).

In the Labrador Sea (Stations 64, 69 and 77), high Ba_{xs} concentrations (> 450 pmol L^{-1} and up to 863 pmol L^{-1} at Station 69) extended to at least 1000 m, without returning to the background level as compared to the other stations outside the Labrador Sea. Results for Go-Flo samples indicated that Ba_{xs} concentrations decreased to the background level (180 pmol L^{-1}) at 1300, 1700 and 1200 m for Stations 64, 69 and 77, respectively.

3.2. Mesopelagic Ba_{xs}

The Ba_{xs} concentrations were integrated (trapezoidal integration) over two depth intervals of the mesopelagic layer (100–500 m and 100–1000 m; Table 2) to obtain depth-weighted average (DWA) Ba_{xs} values.

The DWA Ba_{xs} values between 100 and 500 m ranged from 399 to 672 pmol L^{-1} and from 315 to 727 pmol L^{-1} between 100 and 1000 m (Stations 51 and 69, respectively). The DWA Ba_{xs} values varied by less than a factor of 1.4 between both modes of integration. Only for the Labrador Sea (Stations 64, 69 and 77) the DWA Ba_{xs} values for the 100–1000 m were larger than for the 100-500 m interval. For the latter stations, the Ba_{xs} inventories for the interval between 100 m and the depths were concentrations decreased to background level (1300, 1700 and 1200 m for Go-Flo casts at Stations 64, 69 and 77, respectively) were somewhat smaller than for the inventories between 100–1000 m (up to 1.5

times in the case of Station 77). To facilitate inter-comparison between stations, we consistently considered Ba_{xs} inventories over the 100-1000 m depth interval in the following discussion.

Within the NAST province, Station 13 was characterized by a relatively low DWA Ba_{xs} value of 419 pmol L^{-1}. Similarly, low median DWA Ba_{xs} contents were observed within the NADR province (403 ± 34 pmol L^{-1}, n=4), with the lowest DWA Ba_{xs} observed at Station 26 (391 ± 58 pmol L^{-1}).

The highest median DWA Ba_{xs} value was observed in the ARCT province (566 ± 155 pmol L^{-1}, n=5). There, the DWA Ba_{xs} contents were more variable between stations, ranging from 315 pmol L^{-1} at Station 51 to 727 pmol L^{-1} at Station 69, with a high DWA Ba_{xs} also observed at Station 44 (633 pmol L^{-1}).

4. Discussion

4.1. Barite is the main carrier of Ba_{xs}

Several barite particles were observed associated to or in close proximity to biogenic fragments such as coccoliths (Fig. 3), suggesting they were originally formed inside biogenic microenvironments as proposed by others (Bishop, 1988; Dehairs et al., 1980; Stroobants et al., 1991). However, no barite crystals were observed in the surface waters at Station 26 where very high Ba_{xs} concentrations were recorded (up to 1888 pM), most likely the result of Ba uptake and/or adsorption by biota, as reported by Sternberg et al. (2005) for culture experiments. This result was expected as it fits in the concept of barite formation proposed by Stroobants et al. (1991), showing that the barium sulphate in biogenic aggregates of surface waters is not crystallized, whereas below this surface layer, when organic matter degradation occurs, barite is present as discrete micron-sized particles.

Regarding the contribution of the barite particles to the Ba_{xs} concentration for the sample collected at 600 m of Station 69, we assumed that the small filter portion (only 0.003% of the total filter surface was analysed by FE-SEM) is representative of the whole filter. The Ba concentration deduced from the FE-SEM particle sizing analysis and using Eq. (1) is 1260 pmol L^{-1}. This is in the same order of magnitude, although 1.5 times larger, than the concentration of total Ba_{xs} obtained by ICP-MS (831 pmol L^{-1}) after whole filter digestion. The similarity between both values is remarkable considering the limitations of the FE-SEM procedure (the very small fraction of filter analysed). This also confirms that Ba_{xs} in the mesopelagic layer is carried mostly by barite particles, as observed earlier (Dehairs et al., 1980).

4.2. Factors influencing the DWA Ba_{xs} in the North Atlantic

4.2.1. Influence of the intensity and stage of the bloom

We compared our Ba_{xs} inventories with the average biomass development from January to June 2014 (Fig. 6), which covers the entire productive period in the North Atlantic, starting from winter till the date of our sampling.

Along the GEOVIDE transect, the most productive area was clearly the Labrador Sea of the ARCT province, where Chl-*a* concentrations averaged 6 mg m^{-3} (Fig. 6). This basin was sampled during the decline of the bloom (Fig. 1; Chl-*a* concentration was > 3 mg m^{-3} one month before the sampling, and PP and nutrient concentrations were low during sampling). The high DWA Ba_{xs} observed in this area (Table 2) likely results from the large biological activity during the period preceding sampling. The West European basin of the NADR province, and in particular the area around

Station 21, was also characterized by a high phytoplankton biomass between January and June (Fig. 6), though lower than in the Labrador Sea. Here, the bloom started in May (Fig. 1; Chl-a concentration ≈ 3 mg m^{-3}, one month before the sampling) and was still in progress during the sampling, as indicated by the high PP (135 mmol C m^{-2} d^{-1}). These features can explain the lower DWA Ba_{xs} observed at Station 21 (Table 2) compared to the Labrador Sea. The other stations of the NADR (Stations 26, 32 and 38) were sampled during the bloom development (Fig. 1) with high PP reaching 174 mmol m^{-2} d^{-1} at Station 26. The latter stations were characterized by lower DWA Ba_{xs} values compared to other stations, pointing to a time lag between the phytoplankton bloom and the build-up of the Ba_{xs} signal. However, this was not the case for Station 44, in the Irminger Sea of the ARCT province, which was sampled during the bloom (high PP, high Chl-*a* and high nutrient concentrations during the sampling period) and characterized by one of the highest DWA Ba_{xs}, possibly reflecting an important past bloom.

As also indicated by others, the mesopelagic Ba_{xs} signal builds-up during the growth season and therefore integrates effects of past surface production (Dehairs et al., 1997; Cardinal et al., 2001, 2005). The large regional and temporal variability of the bloom development stage thus results in a large variability of the mesopelagic Ba_{xs} signal in the North Atlantic.

4.2.2. Influence of water masses/physical forcing

The Labrador Sea (Stations 64, 69 and 77) had the largest Ba_{xs} inventory coinciding with the presence of the Labrador Sea Water (LSW; potential temperature between 2.7 and 3.8 °C and salinity below 34.9; Harvey, 1982; Yashayaev, 2007) in the upper 1500 m. The LSW formation takes place in the central Labrador Sea, where convection reached ~1700 m during the winter preceding GEOVIDE (Fig. 2; Kieke and Yashayaev, 2015). The deepening of the mixed layer has been recently shown to represent a major mechanism to convey organic carbon to the mesopelagic zone (from 23 % to > 100 % in high latitude regions; Dall'Olmo et al., 2016), supporting the carbon demand of the mesopelagic food web (Burd et al., 2010; Aristegui et al., 2009). Moreover, the highest mesopelagic prokaryotic heterotrophic abundance during GEOVIDE was observed in the central Labrador Sea (Station 69), reaching 896 cells μL^{-1} at 500 m, while the median values at the other stations for which bacterial cell numbers were available for the mesopelagic zone (Stations 13, 21, 26, 32 and 38), reached only 258 ± 60 cells μL^{-1} at the similar depth (J. Laroche, J. Ratten and R. Barkhouse, personal communication). Therefore, the LSW subduction area appears to reinforce the microbial loop by increasing the layer in which the bacteria can thrive feeding on increased food supplies. This condition appears to increase the Ba_{xs} inventory.

The LSW was also present in the Irminger Sea between 500 and 1000 m at Station 44 (Fig. 2). In the Temperature-Salinity plot, the high Ba_{xs} concentrations of the second peak (823 pmol L^{-1} at 700 m; Fig. 5) are clearly associated with the presence of LSW (Fig. 7a), suggesting that this second deeper Ba_{xs} maximum represents an advected signal. We calculated the DWA Ba_{xs} without taking into account the 2nd peak (100-600 m depth interval) subtracted it from the total DWA Ba_{xs} (100-1000 m depth interval) to estimate the advected signal. At Station 44, the advected Ba_{xs} signal represents some 89 pmol L^{-1}, 14 % of the total signal, which is within the uncertainty of the remineralisation flux calculation (see later below). Similarly, at Station 32 the Temperature-Salinity plot (Fig. 7b) points out that the second Ba_{xs} peak (at 450 m; Fig. 5) was related to the presence of the Subarctic Intermediate water (SAIW; temperature of 5.6 ± 0.1 °C and salinity of 34.70 ± 0.02; Alvarez et al., 2004), which contributes to 14 pmol L^{-1} (3 % of the total signal).

Association of Ba_{xs} maxima with water masses is not always clear, as it is evident from the case of Station 38 where the second Ba_{xs} maximum at 700 m (Fig. 5) does not coincide with a specific water mass (Fig. 7). In this case, the deep Ba_{xs} maximum may possibly result from remineralisation generated by larger or heavier organic aggregates reaching greater depths. At the remaining stations there was no evidence of water mass influence. Overall, lateral transport influencing the local Ba_{xs} distributions was observed at two stations during GEOVIDE but did not significantly modify the magnitude of the local mesopelagic Ba_{xs} inventory. However, the subduction occurring in the Labrador Sea resulted in larger mesopelagic DWA Ba_{xs}, probably due to high organic export and associated prokaryotic heterotrophic activity in these areas.

4.2.3. Influence of the phytoplankton community structure

The different Ba_{xs} inventories may also be influenced by the differences in phytoplankton community compositions. The ARCT province was dominated by diatoms (median value: 63 ± 19 % of the total phytoplankton community taxa; Tonnard et al., 2018, this issue) and was characterized by the highest DWA Ba_{xs} values while the NAST and NADR provinces were characterized by higher abundance of haptophytes (median value: 43 ± 16 % of the total phytoplankton community taxa; Tonnard et al., 2018, this issue) and by lower Ba_{xs} inventories. Coccolithophorids are part of the haptophyte family and their dominance was confirmed by visual observations on filters (surface down to 400 m) by FE-SEM. Calcifiers, such as coccolithophorids, have been shown to be more efficient in transferring carbon to the deep ocean compared to diatoms (Francois et al., 2002; Klaas and Archer, 2002; Lam et al., 2011). This difference could result from the low compaction or the high fluffiness of diatom aggregates, the high degree of degradability of organic compounds within diatom aggregates, the greater density of calcite, the resistance of calcite to grazing and the more refractory nature of the exported organic matter associated to calcite (Bach et al., 2016; Francois et al., 2002; Klaas and Archer, 2002; Lam et al., 2011; Le Moigne et al., 2013a; Ragueneau et al., 2006). Therefore, enhanced particle degradation when diatoms are predominant seems to increase the mesopelagic DWA Ba_{xs}.

4.3. Relationship between Ba_{xs} and carbon remineralisation in the North Atlantic

In previous studies focusing on the Southern Ocean, Ba_{xs} based-mesopelagic carbon remineralisation fluxes were estimated using Eq. (2), which relates the accumulated mesopelagic Ba_{xs} inventory to the rate of oxygen consumption (Shopova et al., 1995; Dehairs et al., 1997):

$$\text{Mesopelagic } Ba_{xs} = 17200 \times JO2 + Ba_{\text{ residual}} \quad (2)$$

where M*esopelagic* Ba_{xs} is the depth-weighted average in the mesopelagic layer (DWA; in pmol L^{-1}), JO_2 is the rate of oxygen consumption (in µmol L^{-1} d^{-1}), and $Ba_{residual}$ is the deep-ocean Ba_{xs} value observed at zero oxygen consumption (or Ba_{xs} background signal), which was determined to reach 180 pmol L^{-1} (Dehairs et al., 1997).

The oxygen consumption JO_2 can be converted into a C remineralisation flux trough Eq. (3):

$$\text{POC mesopelagic remineralisation} = Z \times JO_2 \times (C{:}O_2)_{\text{Redfield Ratio}} \quad (3)$$

where the *POC mesopelagic remineralisation* is in mmol C m^{-2} d^{-1}, *Z* is the thickness of the layer in which the mesopelagic Ba_{xs} is calculated, JO_2 is the rate of oxygen consumption given by Eq. (2) and $(C{:}O_2)_{Redfield\ Ratio}$ is the stoichiometric molar ratio of carbon to dioxygen (127/175; Broecker et al., 1985).

However, it is of interest to investigate if this relationship can be applied in the North Atlantic. Therefore, we determined the oxygen utilization rate (OUR; µmol kg^{-1} yr^{-1}), which is obtained by dividing the apparent oxygen utilization (AOU, in µmol kg^{-1}) by the water mass age (Table S1). From the Iberian coast to Greenland, the age calculation was based on the CFC-12 distribution (when available, otherwise CFC-11) determined in 2012 (OVIDE CARINA cruise, de la Paz et al., 2017). For the Labrador Sea, the mean age of LSW has been estimated by Rhein et al. (2015) based on a 25 year record of CFC contents. The OUR was then integrated over the 100–1000 m layer. The resulting regression between DWA Ba_{xs} and OUR is as follows (see Fig. 8):

$$\text{Mesopelagic } Ba_{xs} = 23391\ (\pm 6368) \times JO_2 + 247\ (\pm 61) \qquad (4)$$

where M*esopelagic* Ba_{xs} and JO_2 are defined in Eq. 2. Here, $Ba_{residual}$ is 247 pmol L^{-1}.

This regression is significant ($R^2 = 0.63$; p-value = 0.006) when Station 44 is excluded. This latter station was located in the Irminger Gyre (Zunino et al., 2017; this issue) and it is possible that the gyre system induced an accumulation and retention of mesopelagic Ba_{xs}, which then no longer reflects remineralisation associated with the present growth season.

Figure 8 also shows the oxygen consumption related to the GEOVIDE Ba_{xs} values using the Southern Ocean regression (Eq. 2). It appears that for a given mesopelagic Ba_{xs} inventory the oxygen consumption is smaller when using the Southern Ocean regression. However, both regressions are not significantly different when taking into account the errors associated with the slope and intercept of the regression in Eq. 4. The Southern Ocean regression appears to represent a lower limit that seems to over-estimate the remineralisation fluxes. Furthermore, the relationship here deduced for the North Atlantic is sensitive to potential errors. Indeed, calculation of OUR has been shown to under-estimate the ocean respiration because of the non-proportional diffusive mixing of AOU and water mass age resulting in an excess loss of AOU versus age (Koeve and Kähler, 2016). This would decrease the mismatch between the Southern Ocean and North Atlantic regressions. Errors can also be directly associated with the CFC-based age values of the water masses, which would appear especially critical for LSW. Indeed, the severe winter preceding the cruise (2013/2014) appeared to have strongly ventilated LSW with a mixed layer depth exceeding 1700 m (Kieke and Yashayaev, 2015), indicating that the mean age (4 years) estimated by Rhein et al. (2015) may have over-estimated the real LSW age (P. Lherminier, personal communication). Moreover, in the Labrador Sea, the residence time of LSW strongly varies between the central Labrador Sea (4–5 years) and the boundary currents off the Greenland and Newfoundland coasts (a few months; Deshayes et al., 2007; Straneo et al., 2003). An over-estimation of these ages leads to under-estimating OUR, resulting in reducing the apparent discrepancy between the both North Atlantic and Southern Ocean regressions.

In the following discussion, carbon remineralisation fluxes are estimated for the North Atlantic (GEOVIDE and GEOSECS cruises) using Eq. (4) and (3).

4.4. Comparison of remineralisation fluxes

4.4.1. Remineralisation from the Ba_{xs} proxy

The GEOVIDE remineralisation fluxes are compared with values reported for the World Ocean and also based on Ba_{xs} inventories (Table 3; Fig. 9). In the North Atlantic, the fluxes obtained during the GEOVIDE and GEOSECS (symbolized by stars in Fig. 9) cruises are of the same order of magnitude, highlighting a relatively constant remineralisation over the last 44 years. The remineralisation fluxes reported for the Southern and Pacific Oceans are similar to those in the NAST and NADR provinces of the North Atlantic. However, the fluxes in the ARCT province are clearly higher, highlighting an important remineralisation in the northern part of the North Atlantic compared to other oceans.

4.4.2. Remineralisation from direct measurements

In the North Atlantic, carbon respiration rates were also deduced from surface drifting sediment traps and associated-shipboard incubations (Fig. 9). Collins et al. (2015) determined very high respiration rates reaching 39 and 72 mmol C m^{-2} d^{-1} at sites located in the NADR and in the ARCT provinces, respectively. Nevertheless, these high fluxes were deduced in the upper mesopelagic layer (50–150 m) where respiration is larger compared to the lower mesopelagic layer (100–1000 m). This difference in depth interval could thus explain the lower remineralisation rates in our study. Also using surface drifting sediment traps and associated-shipboard incubations but supplemented by measurements of zooplankton respiration, Giering et al. (2014) determined respiration rates in the NADR province (PAP site) reaching 7.1 mmol C m^{-2} d^{-1} during summer. This flux, determined over the 50–1000 m depth interval, is of the same order of magnitude as our estimates for the NADR province.

4.4.3. Remineralisation from the deep sediment traps

The remineralisation flux in the mesopelagic layer can also be derived from the difference between a deep POC export flux and a surface POC export flux. Honjo et al. (2008) compiled deep POC fluxes from bottom tethered sediment traps and calculated the corresponding export production (upper-ocean POC export flux) using an ecosystem model (Laws et al., 2000) for most world ocean provinces. Then, by difference, the authors estimated an annual average of carbon remineralisation fluxes in the mesopelagic layer, which were converted into daily average fluxes. Remineralisation fluxes reached values of 34 mmol C m^{-2} d^{-1} in the ARCT province, 9 mmol C m^{-2} d^{-1} in the NADR province and 4 mmol C m^{-2} d^{-1} in the NAST province (Fig. 9). Noteworthy, the flux in the ARCT province was one of the highest mesopelagic remineralisation fluxes estimated worldwide, confirming the occurrence of important remineralisation in the northern part of the North Atlantic as compared to other oceans. The values published by Honjo et al. (2008) for the North Atlantic are quite similar to our median values obtained during GEOVIDE. Indeed, mesopelagic remineralisation fluxes based on the Ba_{xs} proxy were similar to the value reported by Honjo et al. (2008) for the NAST province, while they were respectively 2 and 4 fold lower in the NADR and in the ARCT provinces.
Overall, the remineralisation fluxes deduced from the Ba_{xs} proxy are in concordance with those obtained by the other methods, confirming the order of magnitude of the mesopelagic remineralisation fluxes determined in this study of the North Atlantic (Fig. 9).

4.5. The biological carbon pump in the North Atlantic

In order to investigate the efficiency of the biological carbon pump in the North Atlantic, we examined the daily PP (Fonseca-Batista et al., 2018; this issue; Lemaitre et al., 2018; this issue), the upper-ocean POC export (Lemaitre et al., 2008; this issue) and the POC remineralisation in the mesopelagic layer (Table 3; Fig. 10).

During GEOVIDE, low (≤ 12 %) export efficiencies (i.e., the ratio between PP and POC export) were observed at most stations indicating an accumulation of biomass in surface waters or a strong turn-over of the exported organic matter due to important remineralisation occurring in the upper water column (< 100 m). Furthermore, mesopelagic POC remineralisation fluxes were relatively high, equalling or exceeding the POC export fluxes at some stations. This highlights a strong mesopelagic remineralisation with little or no material left for export to the deep ocean, but above all, it involves an imbalance between carbon supplies and mesopelagic remineralisation.

This imbalance can result from the differences between the time windows over which the PP, POC export and POC remineralisation fluxes are integrated. Indeed, the measurements of PP represent a snapshot (24h incubations) while measurements of export (^{234}Th) integrate several weeks (Benitez-Nelson et al., 2001; Buesseler et al., 1992) and remineralisation (from the Ba_{xs} proxy) probably integrates much longer time scales. Moreover, previous studies in the Southern Ocean showed that mesopelagic processing of exported organic carbon, as reflected by Ba_{xs}, has a phase lag relative to the upper-ocean processes (Dehairs et al., 1997; Cardinal et al., 2005). Thus, we do not expect mesopelagic Ba_{xs} to be in phase with coinciding amplitude of PP and subsequent export. Because of the observed high remineralisation fluxes relative to the export fluxes, particularly in the ARCT province, it is likely that particulate organic matter sank out of the surface waters and became subject to mineralisation in the mesopelagic layer during the period preceding the specific time windows for POC export and PP. Such discrepancies between fluxes can be amplified by the spatial and temporal variability of the phytoplankton blooms in this province, generating sudden high export events and associated remineralisation. In contrast to the above, at Station 32 in the NADR province, a large fraction of exported POC (50%; Table 4), appears to escape remineralisation. The more efficient POC transfer through the mesopelagic layer of this province may be explained by the fact that sampling took place in an early stage of the bloom and/or by the presence of calcified phytoplankton species, ballasting aggregates thereby increasing their settling velocity (see Section 4.1).

Overall, the remineralisation in the mesopelagic layer is an important process that needs to be taken into account as our results point to the poor capacity of specific areas within the North Atlantic to sequester carbon at depths below 1000 m in spring 2014.

5. Conclusion

We investigated mesopelagic carbon remineralisation fluxes in the North Atlantic during the spring 2014 (GEOVIDE section) using for the first time the particulate biogenic barium inventories measured for this area. The excess biogenic barium (Ba_{xs}) inventories in the mesopelagic layer varied between the different provinces of the North Atlantic. The largest Ba_{xs} inventory was observed in the ARCT province, where also high carbon production rates were observed earlier in the season. The regional variations of the Ba_{xs} inventory may also result from differences with phytoplankton community composition encountered along this trans-Atlantic section. Lower mesopelagic Ba_{xs} contents occured where smaller calcified phytoplankton species dominated, such as in the NADR province. Finally, the ARCT province

was also characterized by important water mass subduction, generating a large transport of organic matter to the deep ocean, which might have resulted into an important Ba_{xs} accumulation in the mesopelagic layer.

Using the OUR method, we confirmed that the mesopelagic Ba_{xs} inventory can be related to the oxygen utilisation rate, but the relationship between both parameters is slightly different compared to the relationship proposed elsewhere for the Southern Ocean. A new relationship is thus proposed for the North Atlantic. This proxy approach provided estimations of mesopelagic remineralisation fluxes of similar magnitude as those obtained by others using independent methods (free-floating and moored sediment traps, incubations) in the North Atlantic.

Overall, in spring 2014, the mesopelagic remineralisation balanced or exceeded POC export in the subtropical and subpolar provinces of the North Atlantic, highlighting the important impact of the mesopelagic remineralisation on the biological carbon pump and indicating that little to none organic matter was transferred below 1000 m in this region.

Acknowledgements

We would like to thank the captain and the crew of the R/V Pourquoi Pas?, as well as Fabien Perault and Emmanuel De Saint Léger from the CNRS DT-INSU for their help during the CTD deployments. Pierre Branellec, Floriane Desprez de Gésincourt, Michel Hamon, Catherine Kermabon, Philippe Le Bot, Stéphane Leizour and Olivier Ménage are also acknowledged for their technical help during the cruise. We acknowledge Lorna Foliot, Raphaëlle Sauzède, Joséphine Ras, Hervé Claustre and Céline Dimier for the sampling and analysis of pigments. We would like to thank the co-chief scientists Pascale Lherminier and Géraldine Sarthou. We also express our thanks to Pascale Lherminier, Herlé Mercier, Monika Rhein, Julie Deshayes and Claude Talandier for providing useful help on the characteristics of the Labrador Sea Water. Satellite chlorophyll-a data and visualizations used in this study were produced with the Giovanni and the Ocean Color (Ocean Biology Processing Group; OBPG) online data system, developed and maintained by the NASA.

This work was funded by the Flanders Research Foundation (project G071512N), the Vrije Universiteit Brussel (strategy research program: project SRP-2), the French National Research Agency (ANR-13-BS06-0014 and ANR-12-PDOC-0025-01), the French National Center for Scientific Research (CNRS-LEFE-CYBER), IFREMER and the "Laboratoire d'Excellence" Labex-Mer (ANR-10-LABX-19). For this work, M.I. Garcia-Ibáñez was supported by the Centre for Climate Dynamics at the Bjerknes Centre and by the Spanish Ministry of Economy and Competitiveness through the BOCATS (CTM2013-41048-P) project co-funded by the Fondo Europeo de Desarrollo Regional 2014–2020 (FEDER).

References

Alvarez, M., Pérez, F., Bryden, H. and Rios, A. F.: Physical and biogeochemical transports structure in the North Atlantic subpolar gyre, J. Geophys. Res., 109, 1–21, doi:10.1029/2003JC002015, 2004.

Aristegui, J., Gasol, J. M., Duarte, C. M. and Herndl, G. J.: Microbial oceanography of the dark ocean' s pelagic realm, Limnol. Oceanogr., 54(5), 1501–1529, 2009.

Arístegui, J., Agustí, S., Middelburg, J. J. and Duarte, C. M.: Respiration in the mesopelagic and bathypelagic zones of the oceans, in Respiration in Aquatic Ecosystems, edited by P. A. Del Giorgio and P. J. Williams, pp. 182–206., 2005.

Bach, L. T., Boxhammer, T., Larsen, A., Hildebrandt, N., Schulz, K. G. and Riebesell, U.: Influence of plankton community structure on the sinking velocity of marine aggregates, Global Biogeochem. Cycles, 30, 1145–1165, doi:10.1002/2016GB005372, 2016.

Baltar, F., Aristegui, J., Gasol, J. M., Sintes, E. and Herndl, G. J.: Evidence of prokaryotic metabolism on suspended particulate organic matter in the dark waters of the subtropical North Atlantic, Limnol. Oceanogr., 54(1), 182–193, 2009.
Benitez-Nelson, C., Buesseler, K. O., Karl, D. M. and Andrews, J.: A time-series study of particulate matter export in the North Pacific Subtropical Gyre based on 234 Th : 238 U disequilibrium, Deep Sea Res. Part I Oceanogr. Res. Pap., 48, 2595–2611, 2001.
Bishop, J. K. B.: The barite-opal-organic carbon association in oceanic particulate matter, Nature, 332(6162), 341–343, doi:10.1038/332341a0, 1988.
Boyd, P. W. and Trull, T. W.: Understanding the export of biogenic particles in oceanic waters: Is there consensus?, Prog. Oceanogr., 72(4), 276–312, doi:10.1016/j.pocean.2006.10.007, 2007.
Broecker, W. S., Takahashi, T. and Takahashi, T.: Source and flow patterns of deep ocean, J. Geophys. Res., 90, 6925–6939, doi:10.1029/JC090iC04p06925, 1985.
Buesseler, K. O. and Boyd, P. W.: Shedding light on processes that control particle export and flux attenuation in the twilight zone of the open ocean, Limnol. Oceanogr., 54(4), 1210–1232, doi:10.4319/lo.2009.54.4.1210, 2009.
Buesseler, K. O., Bacon, M. P., Kirk Cochran, J. and Livingston, H. D.: Carbon and nitrogen export during the JGOFS North Atlantic Bloom experiment estimated from 234Th: 238U disequilibria, Deep Sea Res. Part A. Oceanogr. Res. Pap., 39(7–8), 1115–1137, doi:10.1016/0198-0149(92)90060-7, 1992.
Buesseler, K. O., Lamborg, C. H., Boyd, P. W., Lam, P. J., Trull, T. W., Bidigare, R. R., Bishop, J. K. B., Casciotti, K. L., Dehairs, F., Elskens, M., Honda, M., Karl, D. M., Siegel, D. a, Silver, M. W., Steinberg, D. K., Valdes, J., Mooy, B. Van and Wilson, S.: Revisiting Carbon Flux Through the Ocean ' s Twilight Zone, Science (80-.)., 316(April), 567–570, doi:10.1126/science.1137959, 2007.
Burd, A. B., Hansell, D. A., Steinberg, D. K., Anderson, T. R., Aristegui, J., Baltar, F., Beaupré, S. R., Buesseler, K. O., DeHairs, F., Jackson, G. A., Kadko, D. C., Koppelmann, R., Lampitt, R. S., Nagata, T., Reinthaler, T., Robinson, C., Robison, B. H., Tamburini, C. and Tanaka, T.: Assessing the apparent imbalance between geochemical and biochemical indicators of meso- and bathypelagic biological activity: What the @$#! is wrong with present calculations of carbon budgets?, Deep Sea Res. Part II Top. Stud. Oceanogr., 57(16), 1557–1571, doi:10.1016/j.dsr2.2010.02.022, 2010.
Burd, A. B., Buchan, A., Church, M., Landry, M. R., McDonnell, A. M. P., Passow, U., Steinberg, D. K. and Benway, H.: Towards a transformative understanding of the ocean' s biological pump: Priorities for future research, Rep. NSF Biol. Biol. Pump Work., (1–67), doi:10.1575/1912/8263, 2016.
Cardinal, D., Dehairs, F., Cattaldo, T. and André, L.: Geochemistry of suspended particles in the Subantarctic and Polar Frontal zones south of Australia: Constraints on export and advection processes, J. Geophys. Res., 106, 31637, doi:10.1029/2000JC000251, 2001.
Cardinal, D., Savoye, N., Trull, T. W., André, L., Kopczynska, E. E. and Dehairs, F.: Variations of carbon remineralisation in the Southern Ocean illustrated by the Baxs proxy, Deep Sea Res. Part I Oceanogr. Res. Pap., 52(2), 355–370, doi:10.1016/j.dsr.2004.10.002, 2005.
Christaki, U., Lefèvre, D., Georges, C., Colombet, J., Catala, P., Courties, C., Sime-Ngando, T., Blain, S. and Obernosterer, I.: Microbial food web dynamics during spring phytoplankton blooms in the naturally iron-fertilized Kerguelen area (Southern Ocean), Biogeosciences, 11(23), 6739–6753, doi:10.5194/bg-11-6739-2014, 2014.
Collier, R. and Edmond, J.: The trace element geochemistry of marine biogenic particulate matter, Prog. Oceanogr., 13, 113–199, 1984.
Collins, J. R., Edwards, B. R., Thamatrakoln, K., Ossolinski, J. E., Ditullio, G. R., Bidle, K. D., Doney, S. C. and Mooy, B. A. S. Van: The multiple fates of sinking particles in the North Atlantic Ocean, Global Biogeochem. Cycles, 29, 1471–1494, doi:10.1002/2014GB005037, 2015.
Dall'Olmo, G., Dingle, J., Polimene, L., Brewin, R. J. W. and Claustre, H.: Substantial energy input to the mesopelagic ecosystem from the seasonal mixed-layer pump, Nat. Geosci., 1(September), 1–6, doi:10.1038/NGEO2818, 2016.
Daniault, N., Mercier, H., Lherminier, P., Sarafanov, A., Falina, A., Zunino, P., Pérez, F. F., Ríos, A. F., Ferron, B., Huck, T., Thierry, V. and Gladyshev, S.: The northern North Atlantic Ocean mean circulation in the early 21st century, Prog. Oceanogr., 146(July), 142–158, doi:10.1016/j.pocean.2016.06.007, 2016.
Dehairs, F., Chesselet, R. and Jedwab, J.: Discrete suspended particles of barite and the barium cycle in the open ocean, Earth Planet. Sci. Lett., 49, 528–550, 1980.
Dehairs, F., Shopova, D., Ober, S., Veth, C. and Goeyens, L.: Particulate barium stocks and oxygen consumption in the Southern Ocean mesopelagic water column during spring and early summer: Relationship with export production, Deep Sea Res. Part II Top. Stud. Oceanogr., 44(1–2), 497–516, doi:10.1016/S0967-0645(96)00072-0, 1997.
Dehairs, F., Jacquet, S., Savoye, N., Van Mooy, B. a S., Buesseler, K. O., Bishop, J. K. B., Lamborg, C. H., Elskens, M., Baeyens, W., Boyd, P. W., Casciotti, K. L. and Monnin, C.: Barium in twilight zone suspended matter as a potential

proxy for particulate organic carbon remineralization: Results for the North Pacific, Deep Sea Res. Part II Top. Stud. Oceanogr., 55(14–15), 1673–1683, doi:10.1016/j.dsr2.2008.04.020, 2008.
Deshayes, J., Frankignoul, C. and Drange, H.: Formation and export of deep water in the Labrador and Irminger Seas in a GCM, Deep Sea Res. Part I Oceanogr. Res. Pap., 54, 510–532, doi:10.1016/j.dsr.2006.12.014, 2007.
Esaias, W. E., Feldman, G. C., MnClain, C. R. and Elrod, J. A.: Monthly satellite-derived phytoplankton pigment distribution for the North Atlantic basin, Ocenaography Rep., 67(44), 835–837, 1986.
Fernández-Castro, B., Arístegui, J., Anderson, L., Montero, M. F., Hernández-León, S., Maranon, E. and Mourino-Carballido, B.: Mesopelagic respiration near the ESTOC (European Station for Time-Series in the Ocean, 15.5°W, 29.1°N) site inferred from a tracer conservation model, Deep Sea Res. Part I Oceanogr. Res. Pap., 115, 63–73, doi:10.1016/j.dsr.2016.05.010, 2016.
Fonseca-Batista, D., Riou, V., Michotey, V., Fripiat, F., Li, X., Deman, F., Guasco, S., Brion, N., Laroche, J., Elskens, M., Chou, L. and Dehairs, F.: Significant N2 fixation in productive waters of the temperate Northeast Atlantic., Biogeosciences, 2018.
Francois, R., Honjo, S., Krishfield, R. and Manganini, S.: Factors controlling the flux of organic carbon to the bathypelagic zone of the ocean, Global Biogeochem. Cycles, 16(4), 1–20, doi:10.1029/2001GB001722, 2002.
Ganeshram, R. S., François, R., Commeau, J. and Brown-Leger, S. L.: An experimental investigation of barite formation in seawater, Geochim. Cosmochim. Acta, 67(14), 2599–2605, doi:10.1016/S0016-7037(03)00164-9, 2003.
García-Ibáñez, M. I., Pardo, P. C., Carracedo, L. I., Mercier, H., Lherminier, P., Ríos, A. F. and Pérez, F. F.: The water mass structure and transports in the Atlantic Subpolar Gyre, Prog. Oceanogr., 135, 18–36, doi:10.1016/j.pocean.2015.03.009, 2015.
Giering, S. L. C., Sanders, R., Lampitt, R. S., Anderson, T. R., Tamburini, C., Boutrif, M., Zubkov, M. V, Marsay, C. M., Henson, S. A., Saw, K., Cook, K. and Mayor, D. J.: Reconciliation of the carbon budget in the ocean's twilight zone, Nature, 507(7493), 480–483, doi:10.1038/nature13123, 2014.
Gonzalez-Munoz, M. T., Fernandez-Luque, B., Martínez-Ruiz, F., Chekroun, K. Ben, Arias, J. M., Rodríguez-Gallego, M., Martínez-Canamero, M., de Linares, C. and Paytan, A.: Precipitation of barite by Myxococcus xanthus: possible implications for the biogeochemical cycle of barium, Appl. Environ. Microbiol., 69(9), 5722–5725, doi:10.1128/AEM.69.9.5722, 2003.
Gourain, A., Planquette, H., Cheize, M., Menzel, J.-L., Boutorh, J., Shelley, R., Pereira Contraira, L., Lemaitre, N., Lacan, F., Lherminier, P. and Sarthou, G.: Particulate trace metals along the GEOVIDE section, Biogeosciences, 2018.
Harvey, J.: 0-S relationships and water masses in the eastern North Atlantic, Deep Sea Res. Part A. Oceanogr. Res. Pap., 29(8), 1021–1033, 1982.
Henson, S. A., Dunne, J. P. and Sarmiento, J. L.: Decadal variability in North Atlantic phytoplankton blooms, J. Geophys. Res., 114(C4), C04013–C04013, doi:10.1029/2008JC005139, 2009.
Herndl, G. J. and Reinthaler, T.: Microbial control of the dark end of the biological pump, Nat. Geosci., 6(9), 718–724, doi:10.1038/ngeo1921, 2013.
Honjo, S. and Manganini, S. J.: Annual biogenic particle fluxes to the interior of the North Atlantic Ocean; studied at 34°N 21°W and 48°N 21°W, Deep Sea Res. Part I Oceanogr. Res. Pap., 40(1), 587–607, 1993.
Honjo, S., Manganini, S. J., Krishfield, R. A. and Francois, R.: Particulate organic carbon fluxes to the ocean interior and factors controlling the biological pump: A synthesis of global sediment trap programs since 1983, Prog. Oceanogr., 76(3), 217–285, doi:10.1016/j.pocean.2007.11.003, 2008.
Jacquet, S. H. M., Savoye, N., Dehairs, F., Strass, V. H. and Cardinal, D.: Mesopelagic carbon remineralization during the European Iron Fertilization Experiment, Global Biogeochem. Cycles, 22(1), 1–9, doi:10.1029/2006GB002902, 2008a.
Jacquet, S. H. M., Dehairs, F., Savoye, N., Obernosterer, I., Christaki, U., Monnin, C. and Cardinal, D.: Mesopelagic organic carbon remineralization in the Kerguelen Plateau region tracked by biogenic particulate Ba, Deep Sea Res. Part II Top. Stud. Oceanogr., 55(5–7), 868–879, doi:10.1016/j.dsr2.2007.12.038, 2008b.
Jacquet, S. H. M., Dehairs, F., Dumont, I., Becquevort, S., Cavagna, A.-J. and Cardinal, D.: Twilight zone organic carbon remineralization in the Polar Front Zone and Subantarctic Zone south of Tasmania, Deep Sea Res. Part II Top. Stud. Oceanogr., 58(21–22), 2222–2234, doi:10.1016/j.dsr2.2011.05.029, 2011a.
Jacquet, S. H. M., Dehairs, F., Dumont, I., Becquevort, S., Cavagna, A.-J. and Cardinal, D.: Twilight zone organic carbon remineralization in the Polar Front Zone and Subantarctic Zone south of Tasmania, Deep Sea Res. Part II Top. Stud. Oceanogr., 58(21–22), 2222–2234, doi:10.1016/j.dsr2.2011.05.029, 2011b.
Jacquet, S. H. M., Dehairs, F., Cavagna, A. J., Planchon, F., Monin, L., André, L., Closset, I. and Cardinal, D.: Early season mesopelagic carbon remineralization and transfer efficiency in the naturally iron-fertilized Kerguelen area, Biogeosciences, 12, 1713–1731, doi:10.5194/bg-12-1713-2015, 2015.
Kieke, D. and Yashayaev, I.: Studies of Labrador Sea Water formation and variability in the subpolar North Atlantic

611 in the light of international partnership and collaboration, Prog. Oceanogr., 132, 220–232,
612 doi:10.1016/j.pocean.2014.12.010, 2015.
613 Klaas, C. and Archer, D. E.: Association of sinking organic matter with various types of mineral ballast in the deep
614 sea: Implications for the rain ratio, Global Biogeochem. Cycles, 16(4), 1–14, doi:10.1029/2001GB001765, 2002.
615 Koeve, W. and Kähler, P.: Oxygen utilization rate (OUR) underestimates ocean respiration: a model study, Global
616 Biogeochem. Cycles, 30, 1166–1182, doi:10.1002/2015GB005354, 2016.
617 de la Paz, M., García-Ibáñez, M. I., Steinfeldt, R., Ríos, A. F. and Pérez, F. F.: Ventilation versus biology: What is the
618 controlling mechanism of nitrous oxide distribution in the North Atlantic?, Global Biogeochem. Cycles, 31(4), 745–
619 760, doi:10.1002/2016GB005507, 2017.
620 Lam, P. J., Doney, S. C. and Bishop, J. K. B.: The dynamic ocean biological pump: Insights from a global compilation
621 of particulate organic carbon, CaCO3, and opal concentration profiles from the mesopelagic, Global Biogeochem.
622 Cycles, 25(3), 1–14, doi:10.1029/2010GB003868, 2011.
623 Lampitt, R. S. and Antia, A. N.: Particle flux in deep seas: Regional characteristics and temporal variability, Deep Sea
624 Res. Part I Oceanogr. Res. Pap., 44(8), 1377–1403, 1997.
625 Laws, E. A., Ducklow, H. and McCarthy, J. J.: Temperature effects on export production in the open ocean, Global
626 Biogeochem. Cycles, 14(4), 1231–1246, doi:10.1029/1999GB001229, 2000.
627 Lefèvre, D., Guigue, C. and Obernosterer, I.: The metabolic balance at two contrasting sites in the Southern Ocean:
628 The iron-fertilized Kerguelen area and HNLC waters, Deep Sea Res. Part II Top. Stud. Oceanogr., 55, 766–776,
629 doi:10.1016/j.dsr2.2007.12.006, 2008.
630 Lemaitre, N., Planchon, F., Planquette, H., Dehairs, F., Fonseca-Batista, D., Roukaerts, A., Deman, F., Mariez, C. and
631 Sarthou, G.: High variability of export fluxes along the North Atlantic GEOTRACES section GA01 – Part I: Particulate
632 organic carbon export deduced from the 234Th method., Biogeosciences, 2018.
633 Longhurst, A.: Seasonal cycles of pelagic production and consumption, Prog. Oceanogr., 36(95), 77–167, 1995.
634 Longhurst, A. R.: Ecological geography of the sea, Academic P., San Diego., 2010.
635 Martin, J. H., Knauer, G. a., Karl, D. M. and Broenkow, W. W.: VERTEX: carbon cycling in the northeast Pacific,
636 Deep Sea Res. Part A. Oceanogr. Res. Pap., 34(2), 267–285, doi:10.1016/0198-0149(87)90086-0, 1987.
637 Le Moigne, F. A. C., Gallinari, M., Laurenceau, E. and De La Rocha, C. L.: Enhanced rates of particulate organic
638 matter remineralization by microzooplankton are diminished by added ballast minerals, Biogeosciences, 10(9), 5755–
639 5765, doi:10.5194/bg-10-5755-2013, 2013a.
640 Le Moigne, F. A. C., Villa-Alfageme, M., Sanders, R. J., Marsay, C., Henson, S. and García-Tenorio, R.: Export of
641 organic carbon and biominerals derived from 234Th and 210Po at the Porcupine Abyssal Plain, Deep Sea Res. Part I
642 Oceanogr. Res. Pap., 72(August), 88–101, doi:10.1016/j.dsr.2012.10.010, 2013b.
643 Ohnemus, D. C. and Lam, P. J.: Cycling of Lithogenic Marine Particulates in the US GEOTRACES North Atlantic
644 Transect, Deep Sea Res. Part II Top. Stud. Oceanogr., In Press(November 2015), 283–302,
645 doi:http://dx.doi.org/10.1016/j.dsr2.2014.11.019, 2014.
646 Planchon, F., Cavagna, A.-J., Cardinal, D., André, L. and Dehairs, F.: Late summer particulate organic carbon export
647 and twilight zone remineralisation in the Atlantic sector of the Southern Ocean, Biogeosciences, 10(2), 803–820,
648 doi:10.5194/bg-10-803-2013, 2013.
649 Planquette, H. and Sherrell, R. M.: Sampling for particulate trace element determination using water sampling bottles:
650 methodology and comparison to in situ pumps, Limnol. Oceanogr. Methods, 10, 367–388,
651 doi:10.4319/lom.2012.10.367, 2012.
652 Pommier, J., Gosselin, M. and Michel, C.: Size-fractionated phytoplankton production and biomass during the decline
653 of the northwest Atlantic spring bloom, J. Plankton Res., 31(4), 429–446, doi:10.1093/plankt/fbn127, 2009.
654 Ragueneau, O., Schultes, S., Bidle, K., Claquin, P. and Moriceau, B.: Si and C interactions in the world ocean:
655 Importance of ecological processes and implications for the role of diatoms in the biological pump, Global
656 Biogeochem. Cycles, 20(4), n/a-n/a, doi:10.1029/2006GB002688, 2006.
657 Reinthaler, T., van Aken, H., Veth, C., Aristegui, J., Robinson, C., Williams, P. J. B., Lebaron, P. and Herndl, G. J.:
658 Prokaryotic respiration and production in the meso- and bathypelagic realm of the eastern and western North Atlantic
659 basin, Limnol. Oceanogr., 51(3), 1262–1273, 2006.
660 Rhein, M., Kieke, D. and Steinfeldt, R.: Advection of North Atlantic Deep Water from the Labrador Sea to the southern
661 hemisphere, J. Geophys. Res., 120, 2471–2487, doi:10.1002/2014JC010605, 2015.
662 Sabine, C. L., Feely, R. A., Gruber, N., Key, R. M., Lee, K., Bullister, J. L., Wanninkhof, R., Wong, C. S., Wallace,
663 D. W. R., Tilbrook, B., Millero, F. J., Peng, T., Kozyr, A., Ono, T. and Rios, A. F.: The Oceanic Sink for Anthropogenic
664 CO2, Science (80-.)., 305(2004), 367–371, doi:10.1126/science.1097403, 2004.
665 Sanders, R., Henson, S. A., Koski, M., La, C. L. De, Painter, S. C., Poulton, A. J., Riley, J., Salihoglu, B., Visser, A.,
666 Yool, A., Bellerby, R. and Martin, A. P.: The Biological Carbon Pump in the North Atlantic, Prog. Oceanogr., 129,

200–218, doi:10.1016/j.pocean.2014.05.005, 2014.
Schlitzer, R.: Ocean Data View, odv.awi.de, 2017.
Seager, R., Battisti, D. S., Yin, J., Gordon, N., Naik, N., Clement, A. C. and Cane, M. A.: Is the Gulf Stream responsible for Europe's mild winters?, Quartely J. R. Meteorol. Soc., 128, 2563–2586, doi:10.1256/qj.01.128, 2002.
Shopova, D., Dehairs, F. and Baeyens, W.: A simple model of biogeochemical element distribution in the oceanic water column, J. Mar. Syst., 6, 331–344, 1995.
Sigman, D. M. and Boyle, E. A.: Glacial/interglacial variations in atmospheric carbon dioxide, Nature, 407(October), 859–869, 2000.
Sternberg, E., Tang, D., Ho, T. Y., Jeandel, C. and Morel, F. M. M.: Barium uptake and adsorption in diatoms, Geochim. Cosmochim. Acta, 69(11), 2745–2752, doi:10.1016/j.gca.2004.11.026, 2005.
Straneo, F., Pickart, R. S. and Lavender, K.: Spreading of Labrador sea water: an advective-diffusive study based on Lagrangian data, Deep Sea Res. Part A. Oceanogr. Res. Pap., 50, 701–719, doi:10.1016/S0967-0637(03)00057-8, 2003.
Stroobants, N., Dehairs, F., Goeyens, L., Vanderheijden, N. and Van Grieken, R.: Barite formation in the Southern Ocean water, Mar. Chem., 35(1–4), 411–421, doi:10.1016/S0304-4203(09)90033-0, 1991.
Taylor, S. R. and Mclennan, S. M.: The continental crust: its composition and evolution, Blackwells., 1985.
Tonnard, M., Donval, A., Lampert, L., Claustre, H., Ras, J., Dimier, C., Sarthou, G., Planquette, H., van der Merwe, P., Boutorh, J., Cheize, M., Menzel, J.-L., Pereira Contraira, L., Shelley, R., Bowie, A. R., Tréguer, P., Gallinari, M., Duprez de Gesincourt, F., Germain, Y. and Lherminier, P.: Phytoplankton assemblages along the GEOVIDE section (GEOTRACES section GA01) using CHEMTAX, Biogeosciences, 2018.
Volk, T. and Hoffert, M. I.: Ocean carbon pumps: analysis of relative strengths and efficiencies in ocean-driven atmospheric CO2 changes, in The carbon cycle and atmospheric CO2: Natural variations Archean to Present, vol. 32, pp. 99–110., 1985.
Yashayaev, I.: Hydrographic changes in the Labrador Sea, 1960-2005, Prog. Oceanogr., 73, 242–276, doi:10.1016/j.pocean.2007.04.015, 2007.
Zunino, P., Lherminier, P., Mercier, H., Daniault, N., García-Ibáñez, M. I. and Pérez, F. F.: The GEOVIDE cruise in May-June 2014 reveals an intense Meridional Overturning Circulation over a cold and fresh subpolar North Atlantic, Biogeosciences, 14(23), 5323–5342, doi:10.5194/bg-14-5323-2017, 2017.

Table 1: **Particulate Barium (Ba) and Aluminium (Al) concentrations and resulting recoveries of the certified reference materials SLRS-5 (river water), BHVO-1 (basalt powder), JB-3 (basalt powder) and JGb-1 (gabbro powder).**

	Ba	Al
SLRS-5 (µg kg^{-1})	13 ± 1	47 ± 2
n=4	95 %	95 %
BHVO-1 (µg g^{-1})	129 ± 1	70118 ± 984
n=4	93 %	96 %
JB-3 (µg g^{-1})	229 ± 13	92144 ± 1620
n=4	94 %	101 %
JGb-1 (µg g^{-1})	68 ± 15	91491 ± 732
n=4	106 %	99 %

Table 2: **Depth-weighted average (DWA) values of mesopelagic Ba_{xs} (in pmol L^{-1}) for the 100–500 m and 100–1000 m depth intervals. The biogeochemical provinces defined by Longhurst et al. (1995) are also indicated: NAST: North Atlantic subtropical gyre; NADR: North Atlantic drift; ARCT: Atlantic Arctic.**

Province	Station	Latitude (° N)	Longitude (° E)	DWA Ba_{xs} 100-500 m (pmol L^{-1})			DWA Ba_{xs} 100-1000 m (pmol L^{-1})		
NAST	13	41.4	-13.9	578	±	89	419	±	71
NADR	21	46.5	-19.7	428	±	69	394	±	64
	26	50.3	-22.6	405	±	59	391	±	58
	32	55.5	-26.7	522	±	81	413	±	66
	38	58.8	-31.3	572	±	86	465	±	78
ARCT	44	59.6	-38.9	678	±	104	633	±	98
	51	59.8	-42	399	±	72	315	±	58
	64	59.1	-46.1	464	±	95	566	±	99
	69	55.8	-48.1	672	±	111	727	±	118
	77	53	-51.1	472	±	80	505	±	83

Table 3: **Comparison of the Ba_{xs} inventory (pmol L^{-1}) and related-carbon mesopelagic remineralisation fluxes (mmol C m^{-2} d^{-1}) obtained in the World Ocean. Fluxes are calculated with the new North Atlantic regression (Eq. 4) for the GEOVIDE and GEOSECS cruises and with the Southern Ocean regression (Eq. 2) for the other studies. HNLC: High Nutrient-Low Chlorophyll; art. Fe-fertilized: artificially Fe-fertilized; nat. Fe-fertilized: naturally Fe-fertilized; PF: Polar Front; NAST: North Atlantic subtropical gyre; NADR: North Atlantic drift; ARCT: Atlantic Arctic.**

Cruise (season)	Location	Features	Depth interval, m	DWA Ba_{xs} pmol L^{-1}	MR fluxes mmol C m^{-2} d^{-1}	Reference
CLIVAR SR3 - SAZ98 (spring/summer)	Australian sector Southern Ocean	spring summer	150 - 400	235 - 554 296 - 353	0.3 - 3.0 0.2 - 3.4	Cardinal et al., 2005
VERTIGO (summer)	Pacific Ocean	oligotrophic (Aloha station) mesotrophic (K2 station)	150 - 500	157 - 205 367 - 713	1.0 - 3.0 2.7 - 8.8	Dehairs et al., 2008
EIFEX (summer)	Atlantic sector Southern Ocean	art. Fe-fertilized (in patch) HNLC (out patch)	150 - 1000	273 - 415 233 - 423	2.6 - 7.7 1.2 - 8.0	Jacquet et al., 2008a
KEOPS (summer)	Indian sector Southern Ocean	nat. Fe-fertilized (A3 station) HNLC (C11 station)	125 - 450	342 - 401 309 - 493	2.1 - 2.8 1.7 - 4.0	Jacquet et al., 2008b
SAZ-SENSE (summer)	Australian sector Southern Ocean	nat. Fe-fertilized (SAZ east) HNLC (SAZ west)	100 - 600	244 - 395 199 - 249	3.0 - 6.1 2.1 - 3.1	Jacquet et al., 2011
Bonus GoodHope (summer)	Atlantic sector Southern Ocean	North of PF South of PF	125 - 600	284 - 497 235 - 277	2.1 -6.4 1.1 - 1.9	Planchon et al., 2013
KEOPS 2 (spring)	Indian sector Southern Ocean	nat. Fe-fertilized (A3 station) HNLC (R2 station)	150 - 400	267 - 314 572	0.9 - 1.2 4.2	Jacquet et al., 2015
GEOSECS II (summer)	North Atlantic	NAST+NADR ARCT	100 - 1000	199 - 361 242 - 413	0.5 - 4.9 1.7 - 6.3	Brewer (unpublished values)
GEOVIDE (spring)	**North Atlantic**	**NAST (station 13)** **NADR (station 21)** **NADR (station 26)** **NADR (station 32)** **NADR (station 38)** **ARCT (station 44)** **ARCT (station 51)** **ARCT (station 64)** **ARCT (station 69)** **ARCT (station 77)**	**100 - 1000**	**419** **394** **391** **413** **465** **633** **315** **566** **727** **505**	**4.6** **3.9** **3.8** **4.4** **5.9** **10** **1.8** **8.6** **13** **6.9**	**this study**

728 **<u>Table 4:</u> Comparison of the mesopelagic POC remineralisation fluxes (Remineralisation) with primary production (PP)**
729 **and POC export fluxes in the upper water column (Export). All fluxes are expressed in mmol C m^{-2} d^{-1}. [1] PP data from**
730 **Fonseca-Batista et al. (2018; this issue) and Lemaitre et al. (2018; this issue); [2] Export data from Lemaitre et al. (2018;**
731 **this issue).**

732

	ARCT - Labrador Sea			*ARCT - Irminger Sea*		*NADR*				*NAST*
Station	77	69	64	51	44	38	32	26	21	13
PP [1]	95	31	67	165	137	68	142	174	135	80
Export [2]	6	10	8	3	1	5	8	7	5	2
Remineralisation	7	13	9	2	10	6	4	4	4	5

733

734

735

736

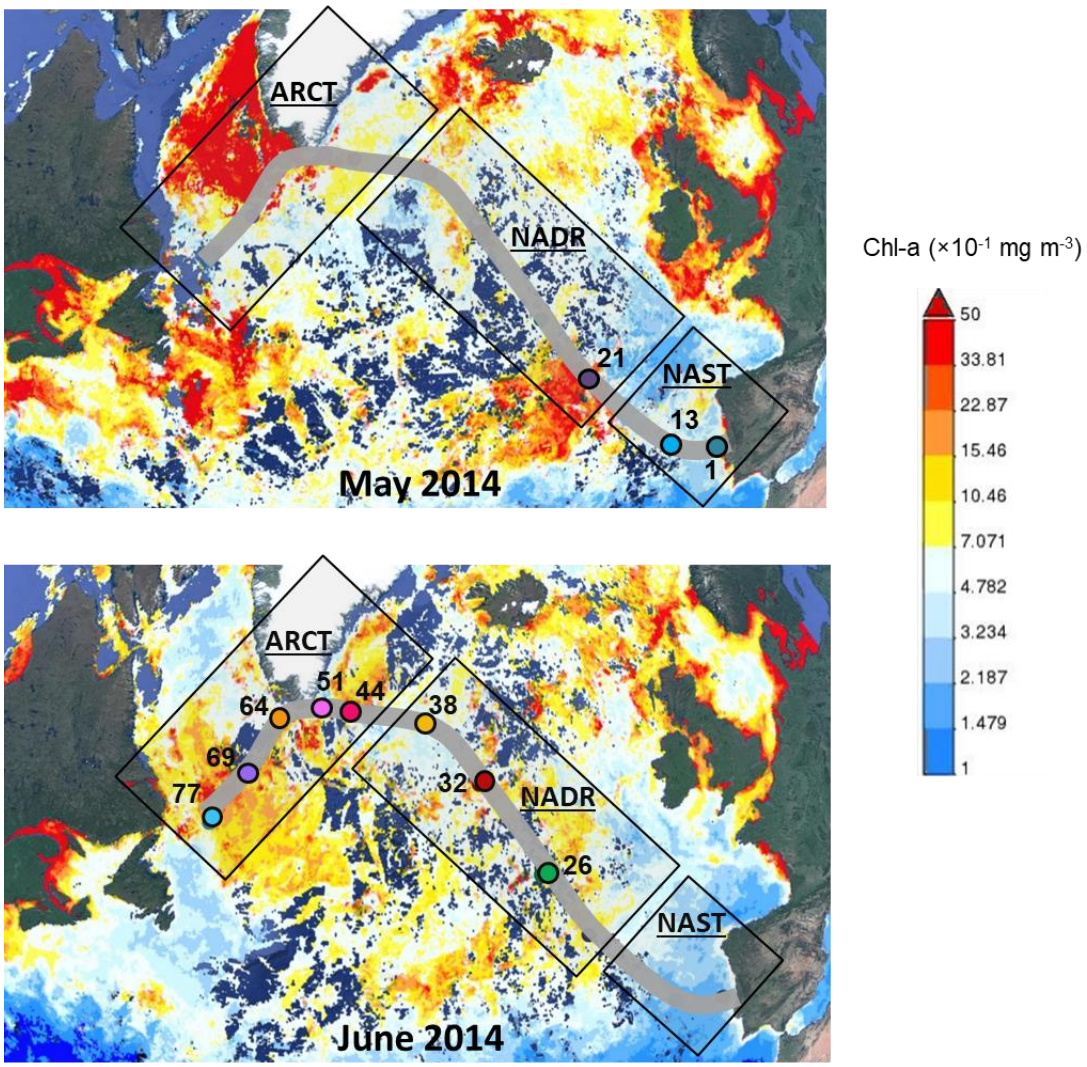

Figure 1: **Satellite derived Chlorophyll-*a* concentrations (MODIS Aqua from http://giovanni.sci.gsfc.nasa.gov/), in mg m^{-3} during the GEOVIDE cruise (May and June 2014). The GEOVIDE transect (grey line) and the main crossed provinces are indicated. NAST: North Atlantic Subtropical gyre; NADR: North Atlantic Drift; ARCT: Atlantic Arctic. Coloured circles indicate stations sampled at the corresponding month.**

(a)

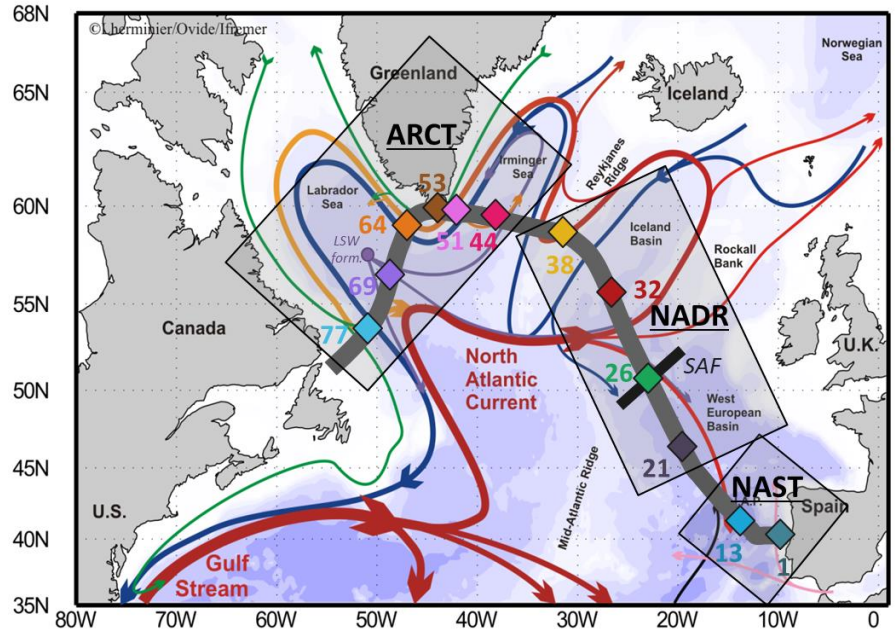

(b)

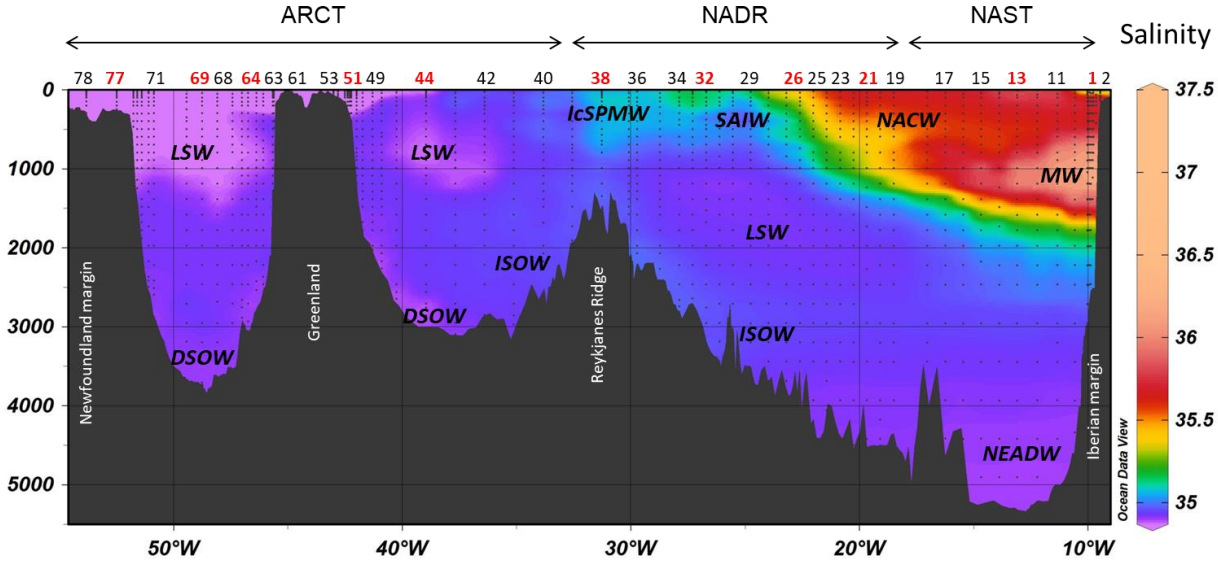

Figure 2: (a) Schematic of the circulation features, adapted from García-Ibáñez et al. (2015). Bathymetry is plotted in colour with interval boundaries at 100 m, at 1000 m and every 1000 m below 1000 m. The red and green arrows represent the main surface currents, the pink and orange arrows represent currents at intermediate depths and the blue and purple arrows represent the deep currents. Diamonds indicate station positions. The approximate locations of the sub-arctic front (SAF; black bar crossing Station 26) and the formation site of the Labrador Seawater (LSW form.) are indicated. (b) Salinity along the GEOVIDE section, and associated water masses: LSW: Labrador Sea Water; ISOW: Iceland–Scotland Overflow Water; IcSPMW: Iceland Subpolar Mode Water; SAIW: Subarctic Intermediate Water; NACW: North Atlantic Central Waters; MW: Mediterranean Water; DSOW: Denmark Strait Overflow Water; NEADW: North East Atlantic Deep Water. Station labels in red indicate sites where Niskin casts were sampled. NAST: North Atlantic Subtropical gyre; NADR: North Atlantic Drift; ARCT: Atlantic Arctic. Data were plotted using ODV software (Schlitzer, 2017).

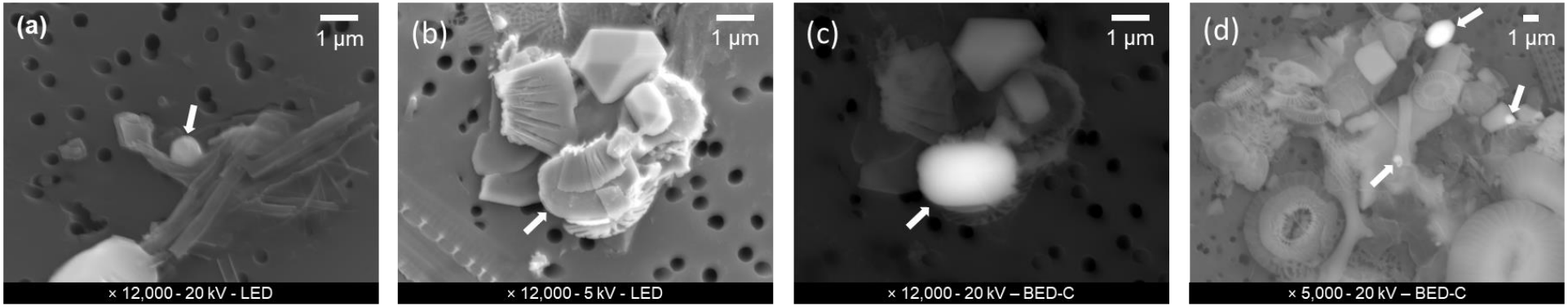

Figure 3: **Barite particles observed by FE-SEM at (a) Station 38 (300 m); (b and c) Station 44 (700 m); (d) Station 69 (600 m). (c) is the backscattered electron image of the aggregate in (b) highlighting the shape of the partly hidden barite crystal. White arrows indicate the position of barite crystals.**

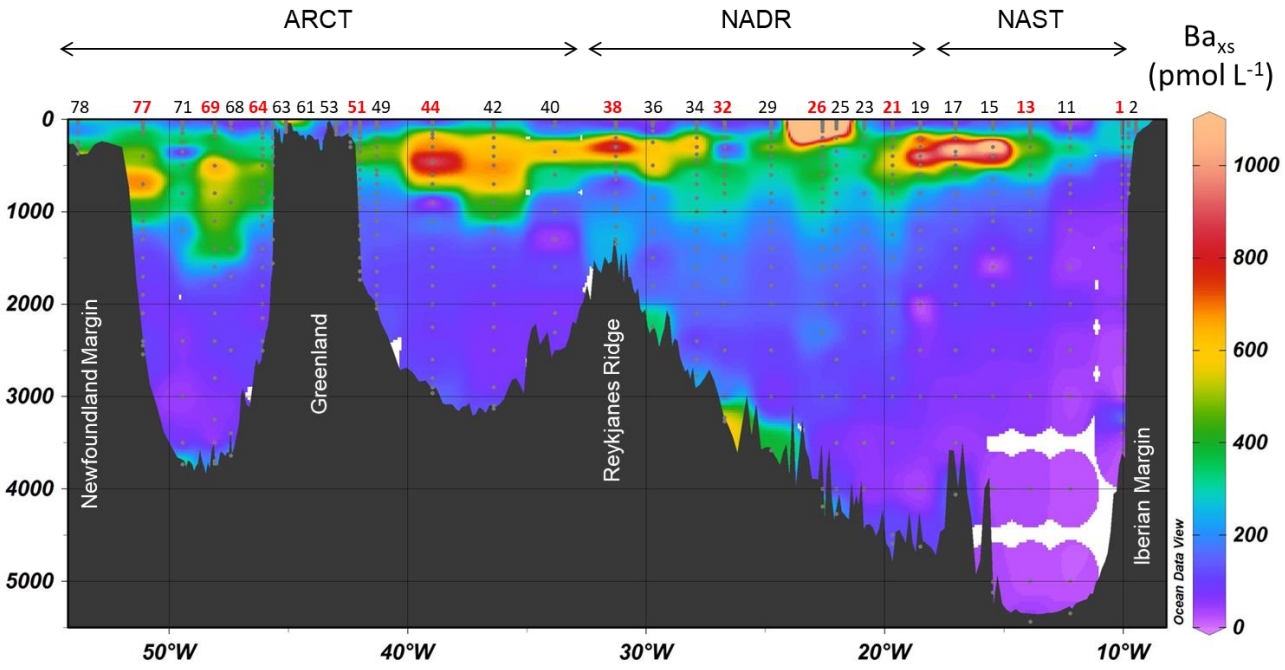

772

773 **<u>Figure 4:</u> Section of the particulate biogenic barium (Ba_{xs}) in pmol L^{-1} determined in samples collected with the Go-Flo**
774 **bottles. Stations labelled in red are those where profiles were also obtained from Niskin casts. Data were plotted using the**
775 **ODV software (Schlitzer, 2017).**

776

777

778

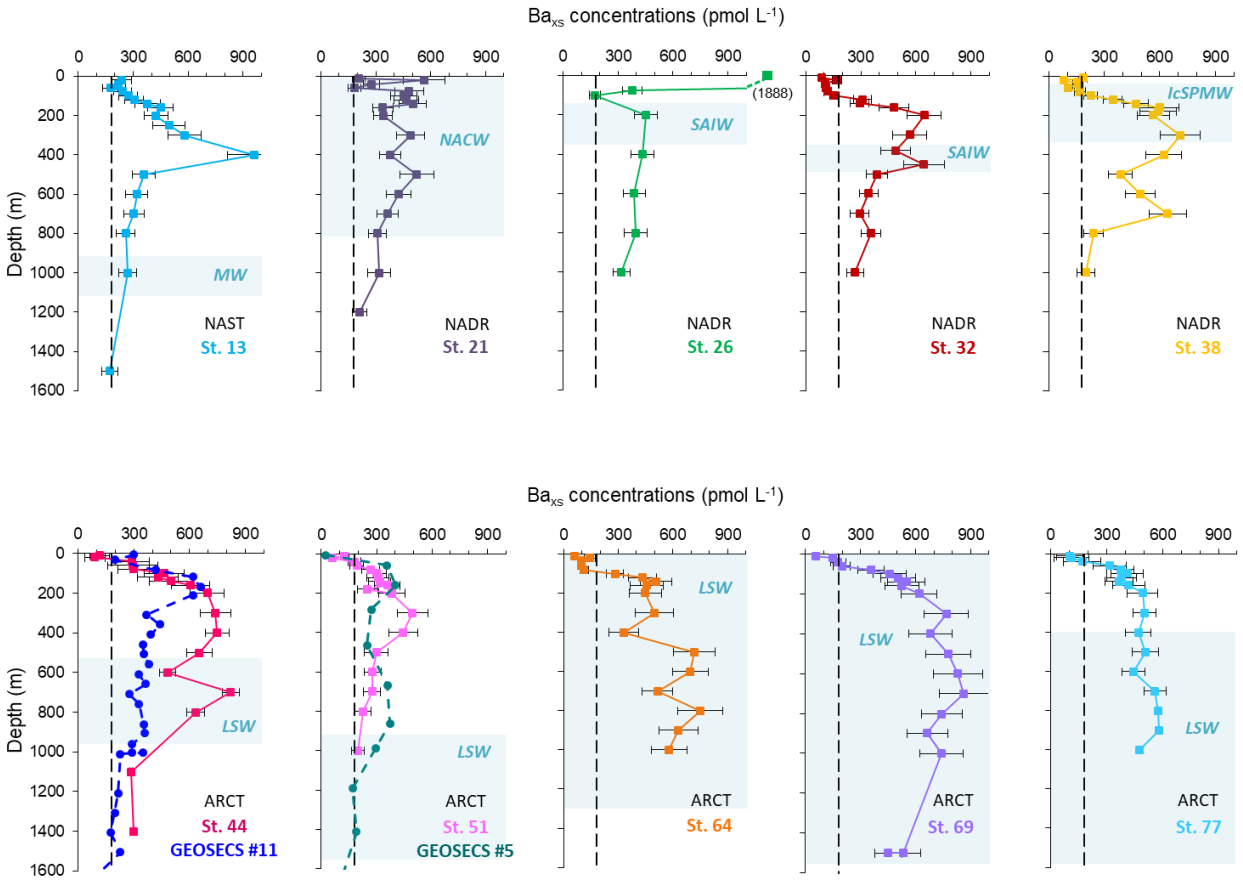

<u>Figure 5:</u> Vertical profiles of Ba_{xs} concentrations (in pmol L^{-1}) determined from Niskin casts during GEOVIDE (squares) and GEOSECS (circles) cruises. The vertical black dashed line (at 180 pmol L^{-1}) represents the deep-ocean Ba_{xs} value (or Ba_{xs} background signal; Dehairs et al., 1997). The approximate depth range of the major water masses is also indicated in blue shading.

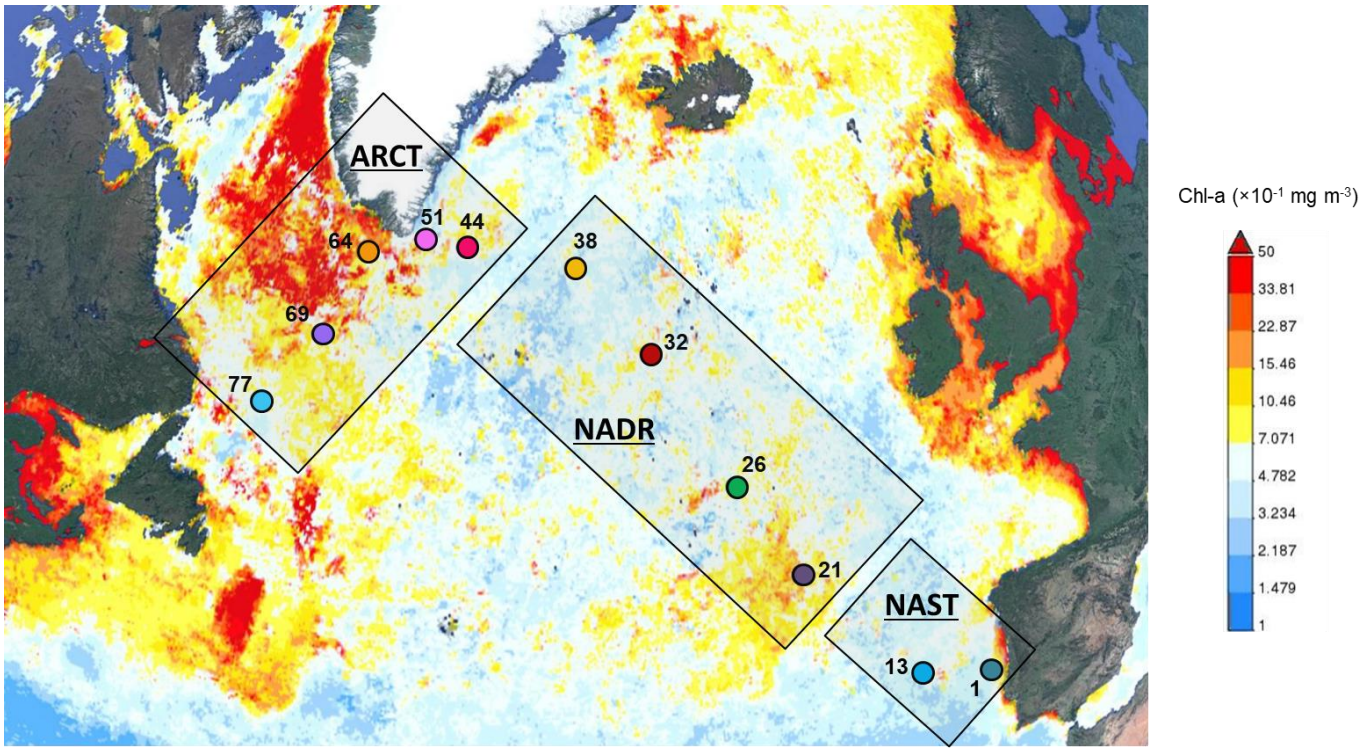

785

786 **Figure 6: Map of time averaged Chlorophyll-*a* concentrations (in mg m^{-3}) for the period from January to June 2014 (monthly**
787 **4 km MODIS Aqua model; http://giovanni.sci.gsfc.nasa.gov/).**

788

789

790

791

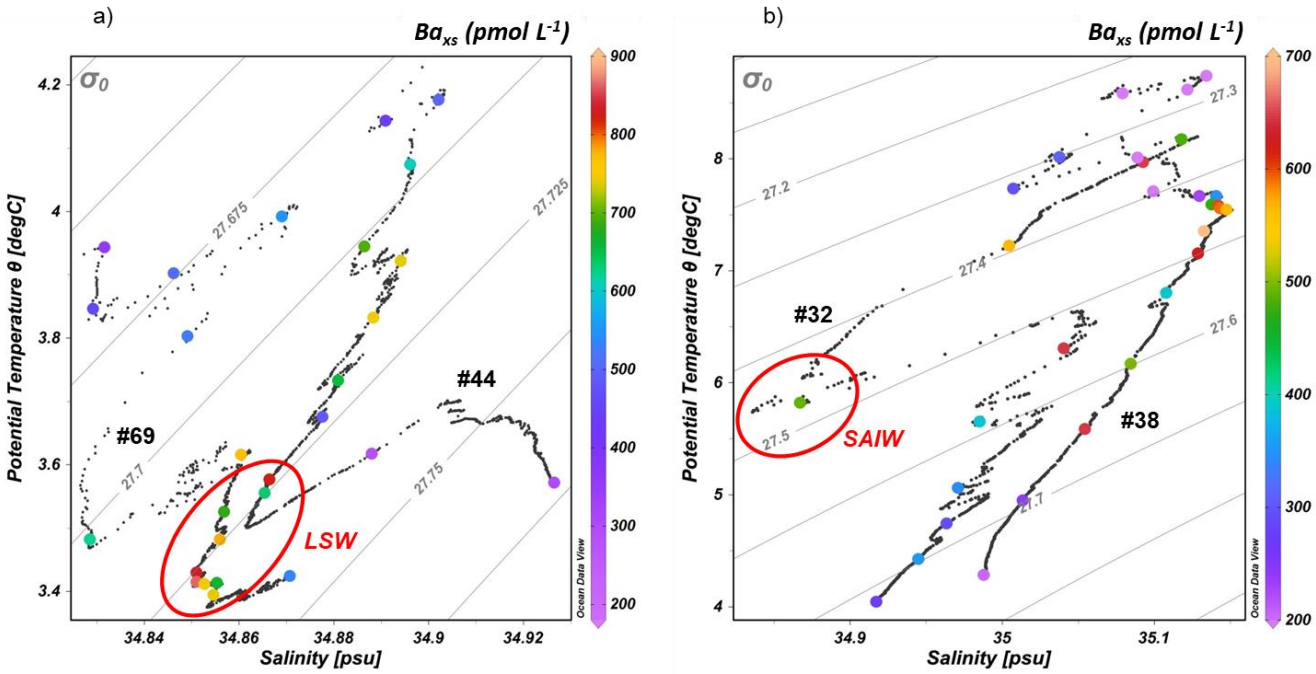

<u>Figure 7:</u> Potential temperature θ - salinity plots with isopycnals for Stations (a) #44 and #69 and (b) #32 and #38 of the GEOVIDE cruise, with focus on the 50–2000 m depth interval. Coloured dots represent the discrete samples analysed for Ba_{xs} with concentration scale on the right. LSW: Labrador Sea Water; SAIW: Subarctic Intermediate Water. Data were plotted using the ODV software (Schlitzer, 2017).

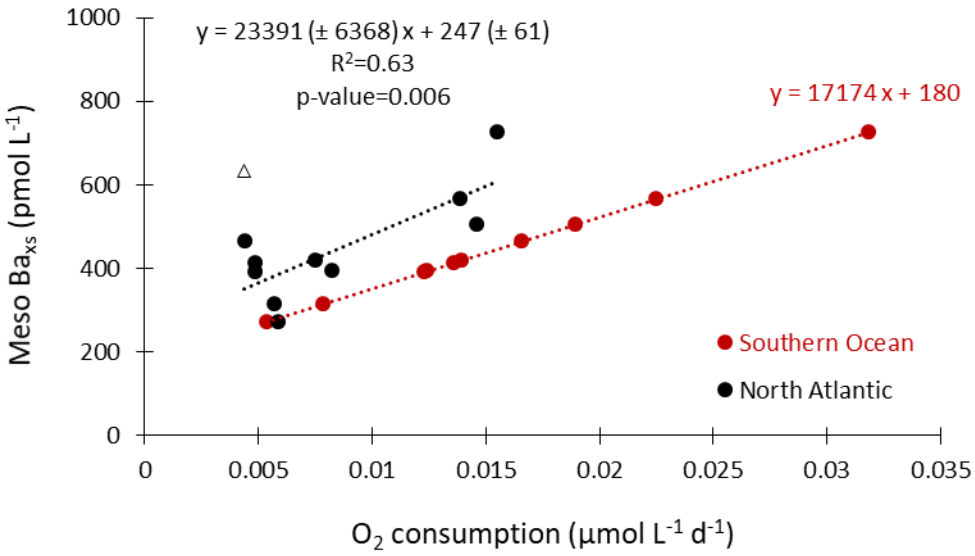

Figure 8: **Regression of DWA mesopelagic Ba_{xs} (pmol L^{-1}) versus O_2 consumption rate (µmol L^{-1} d^{-1}) using the Southern Ocean transfer function from Dehairs et al. (1997; red circles) and the transfer function obtained here for the North Atlantic (black circles). Station 44 (triangle) was excluded from the regression. If station 44 is included, R^2=0.33 and p-value= 0.07.**

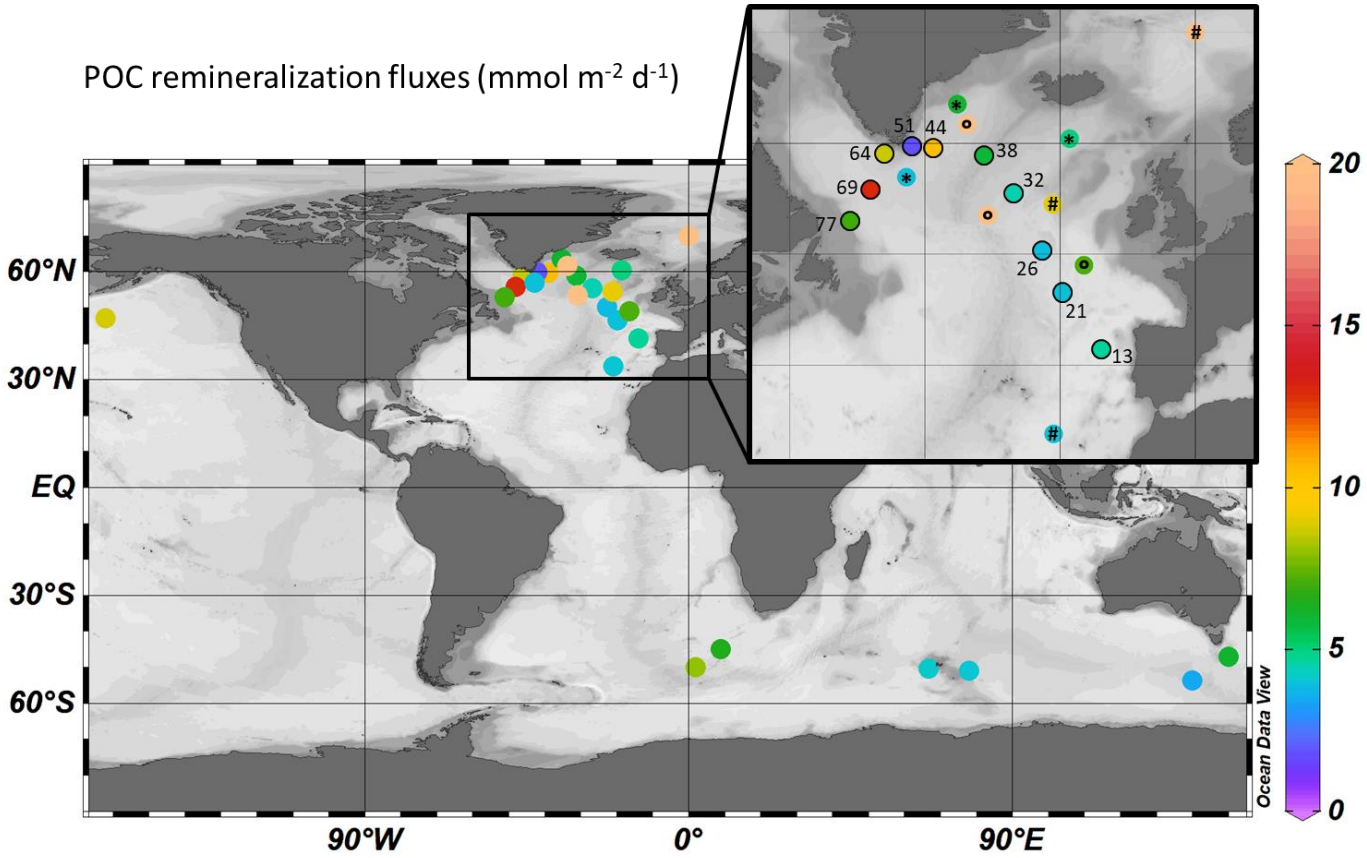

Figure 9: **Summary of published POC remineralisation fluxes (in mmol C m^{-2} d^{-1}) in the World's Ocean. The remineralisation fluxes for the Pacific Ocean (Dehairs et al., 2008) and the Southern Ocean (Cardinal et al., 2005; Jacquet et al., 2008a, 2008b, 2011b, 2015; Planchon et al., 2013) were calculated based on the Ba_{xs} inventories. Insert shows data for the North Atlantic: sites indicated by circles lined in black are from the present study; at sites labelled with # symbols remineralisation was deduced from POC fluxes recorded by moored sediment traps (Honjo et al., 2008); at sites labelled by ° remineralisation was obtained from on-board incubations (Collins et al., 2015; Giering et al., 2014); sites labelled with * are GEOSECS sites for which we calculated remineralisation from existing Ba_{xs} profiles (Brewer et al., unpublished results). Data were plotted using the ODV software (Schlitzer, 2017).**

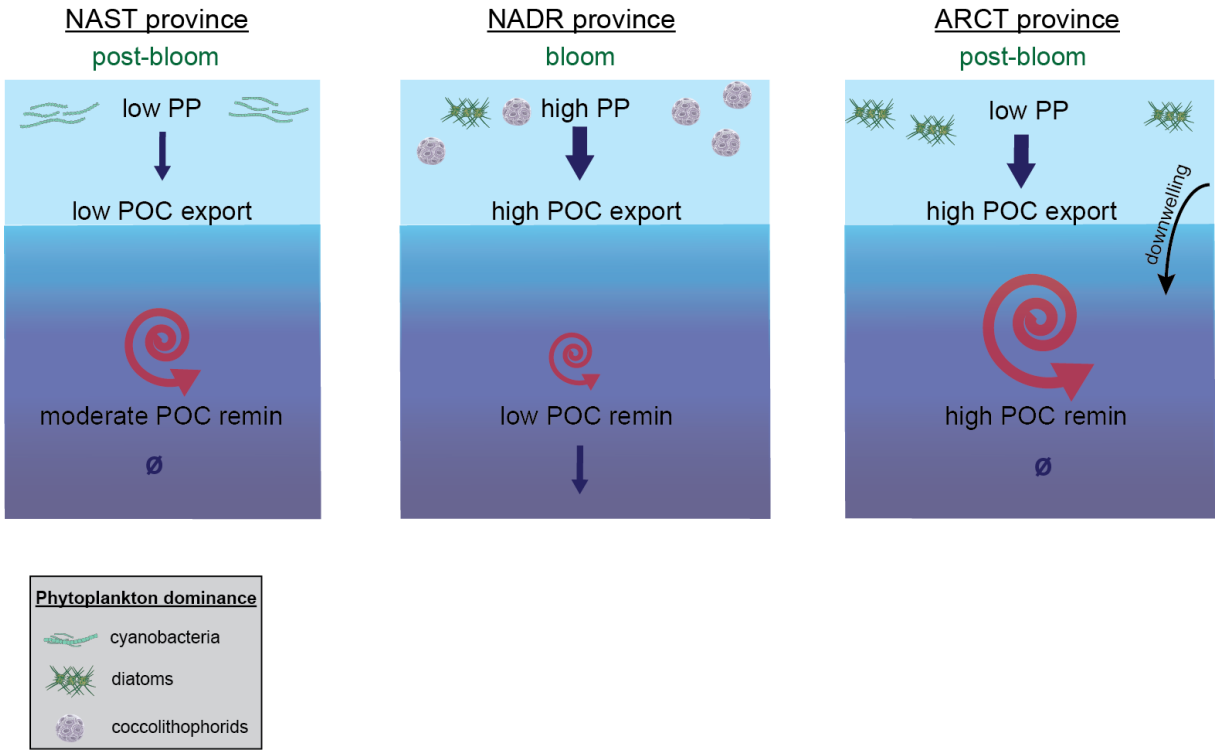

822
823

824 **Figure 10: General schematic of the biological carbon pump in the NAST, NADR and ARCT provinces during GEOVIDE.**
825 **Primary production (PP) data from Fonseca-Batista et al. (2018; this issue) and Lemaitre et al. (2018; this issue); particulate**
826 **organic carbon (POC) export fluxes from Lemaitre et al. (2018; this issue) and POC remineralisation fluxes from this study.**
827 **The dominating phytoplankton communities and the stage of the bloom are also indicated.**

828